Supporting Information

Hydrogen production via aqueous-phase reforming of methanol catalyzed by ruthenium(II) complexes with Schiff-base pincer ligands

Chong Ma,[a,‡] Yihao Xia,[a,‡] Xue Ding,[a] Lei Qin[a,b] and Zhiping Zheng*[a,b]*

[a] Department of Chemistry, Southern University of Science and Technology, Shenzhen, Guangdong, 518055, China.

[b] Shenzhen Grubbs Institute and Guangdong Provincial Key Laboratory of Catalysis, Southern University of Science and Technology, Shenzhen, 518055, China

[‡] These authors contributed equally to this work.

Contents

1. General procedures.

^{1}H and ^{31}P NMR spectroscopy were recorded using Bruker Ascend™ 400 MHz spectrometers. All NMR data are expressed as chemical shifts in ppm. ^{1}H and ^{13}C NMR chemical shifts were determined relative to the internal standard $CHCl_3$ (7.26 ppm and 77.16 ppm, respectively) in $CDCl_3$, DMSO (2.50 ppm and 39.52 ppm, respectively) in *d*$_6$-DMSO or H_2O (4.79 ppm) in D_2O. ^{31}P NMR spectra were calibrated with an external H_3PO_4 standard (0 ppm). NMR spectra were interpreted and processed using MestReNova. Quantitative gas measurements were performed using a burette (500 mL or 1000 mL). Gas chromatography analyses were performed on an Agilent Technologies 7820A gas chromatograph with Ar carrier gas. The gas integration was calibrated using a single-point method by certified gas mixtures from commercial suppliers (Huateshen company) with the following gas volume: H_2 (10%), CO (10 ppm), CH_4 (1%), CO_2 (1%). Elemental analyses were performed on an Elementar vario EL cube element analyzer. Fourier transform infrared (FT-IR) spectra were recorded on a Vertex 80 spectrometer. The single-crystal data of **C3** and **C4** were collected on a Bruker D8 VENTURE CCD diffractometer, using graphite monochromated Mo *K*α radiation (λ = 0.71073 Å). Cell parameters, data reduction, and absorption corrections were performed using Bruker SAINT and SADABS. Using Olex2,[S1] the structure was solved with the SHELXS[S2] structure solution program using direct methods and refined with the SHELXL[S3] refinement package using least squares minimization. All non-H atoms were refined anisotropic Ally.

Calculation of the hydrogen volume and TON. For the experiment data obtained using a gas burette, the turnover number (TON) was calculated based on the amount of hydrogen gas, meaning each produced hydrogen molecule represents one turnover number. In detail, the TON was calculated using the following equation:

$$TON = \frac{V_{obsved} - V_{blank}}{V_{m,H_2,22^oC} * n_{cat}}$$

V_{obs}: measured gas volume from gas burette (mL)

V_{blank}: the blank volume (mL)

n_{cat}: amount of catalyst (mmol)

$V_{m,H_2,22^oC}$: molar gas volume, $V_{m,H_2,22^oC}$ = 24.2 mL/mmol at 22 °C calculated from the Van der Waals Equation:

$$V_{m,H_2,22^oC} = \frac{RT}{p} + b - \frac{a}{RT} = 24.2\frac{mL}{mmol}$$

For hydrogen gas, the parameters are R = 8.3145 m^3 Pa·mol^{-1}·K^{-1}, T = 298.15 K, p = 101325 Pa, a = 2.49·10^{-10} Pa·m^3·mol^{-2}, b = 26.7·10^{-6} m^3·mol^{-1}.

General procedures for aqueous-phase methanol reforming (APMR) dehydrogenation reaction and gas composition analysis. All the experiments were conducted under Ar atmosphere. A mixture of MeOH/H_2O (10 mL) or pure methanol (10 mL) was added to a given amount of base, and the resulting solution was degassed with Ar gas before the following procedure. Then, the catalyst was added, and the mixture was rapidly heated to the target temperature. The gas evolution values $V_{observed}$ were measured by 1000 mL or 500 mL gas burette. Moreover, the corresponding blank values V_{blank} were also calculated without the addition of catalyst. The difference ($V_{observed} - V_{blank}$) is the volume of the gas generated due to the action of the catalyst. After a certain reaction time, 1 mL of gas was extracted for the GC test to confirm the gas composition and the ratio of different compositions.

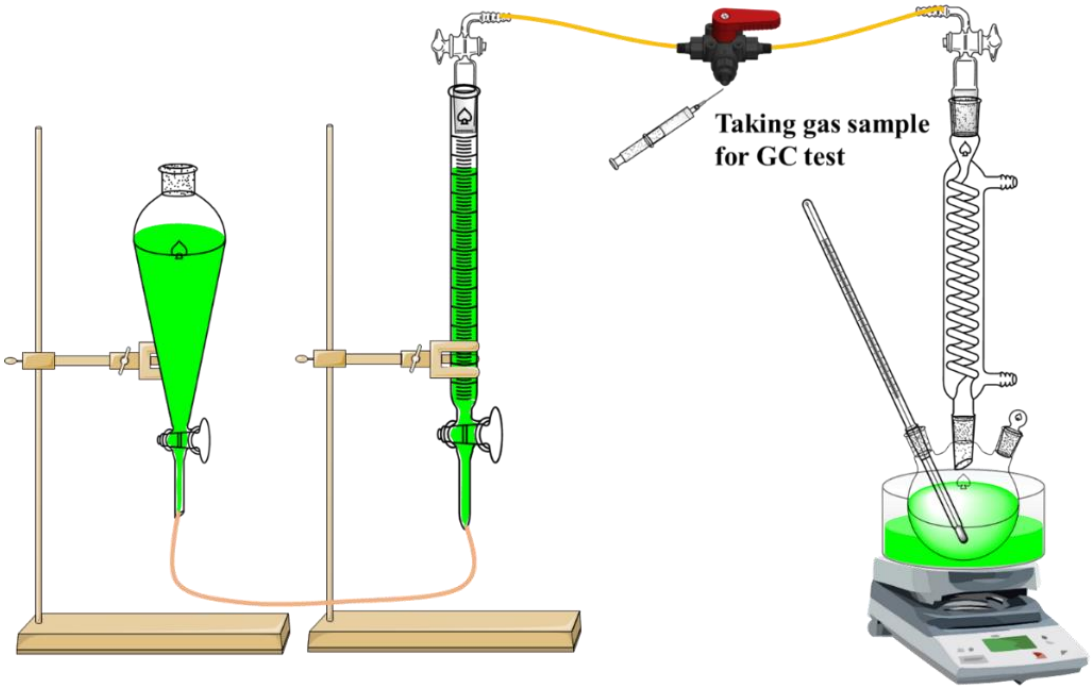

Figure S1. The schematic presentation of the reaction apparatus.

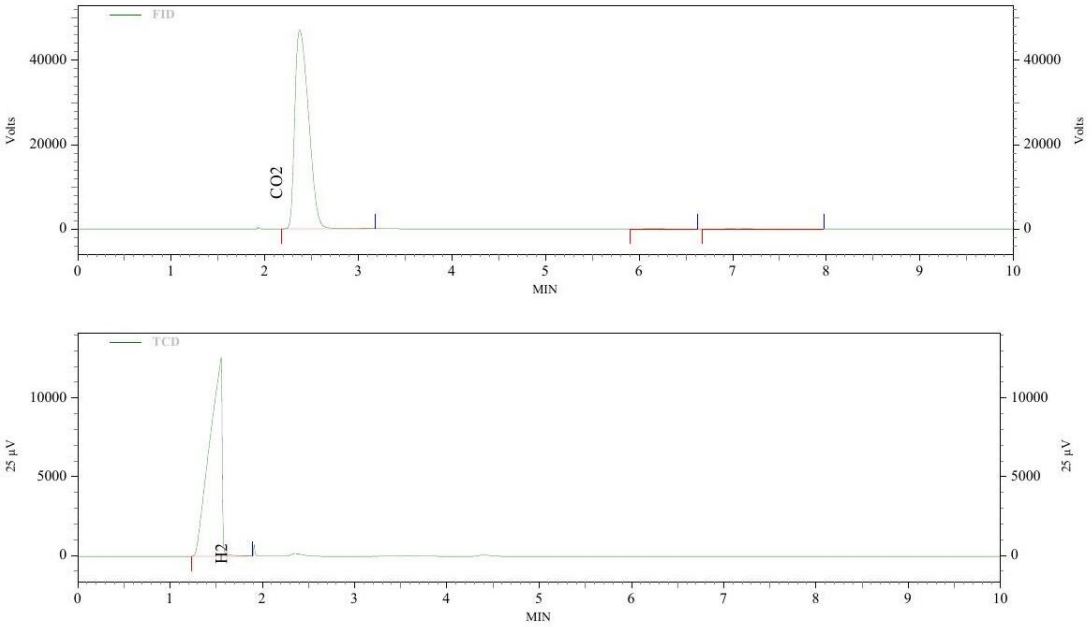

FID result

Peak #	Name	Retention	Area	Amount %
	CO2	2.443	54745305	**0.101**
	CH4			**0.000 BDL**
3	CO			**0.000 BDL**
Total			54745305	**0.101**

TCD result

Peak #	Name	Retention	Area	Amount %
1	H2	1.557	912556803	**56.409**
Total			912556803	**56.409**

Figure S2. GC analysis of the gas mixture from the aqueous-phase reforming of methanol catalyzed by **C4**. Reaction conditions: n_{cat} = 3 μmol, n_{KOH} = 80 mmol, T_{set} = 130 ºC, V = 10 mL (MeOH/H_2O = 9/1, v/v).

2. Synthesis and Characterization

2.1 Synthesis of Pyridine-2,6-dicarbaldehyde.

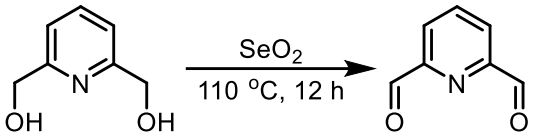

Pyridine-2,6-dicarbaldehyde was synthesized according to a method described in the literature.[S4] SeO_2 (1.11 g, 10 mmol) was added to pyridine-2,6-diyldimethanol (1.39 g, 10 mmol) in dioxane (50 mL) under an argon atmosphere. The reaction mixture was refluxed with stirring at 100 °C for 12 hours. After completion, the solvent was removed via rotary evaporation. The residue was dissolved in minimal chloroform and eluted through a short silica gel column. The crystalline light brown 2,6-pyridinedicarboxaldehyde (1.15 g, 85% yield) was isolated after the evaporation of ethyl acetate. Anal. Calc. for $C_7H_5NO_2$: C, 62.22; H, 3.73; N, 10.37. Found: C, 62.31; H, 3.75; N, 10.22. ^{1}H NMR (400 MHz, $CDCl_3$) δ 10.17 (s, 2H), 8.21−8.15 (m, 2H), 8.13−8.04 (m, 1H). ^{13}C NMR (101 MHz, $CDCl_3$) δ 192.36, 153.03, 138.40, 125.34.

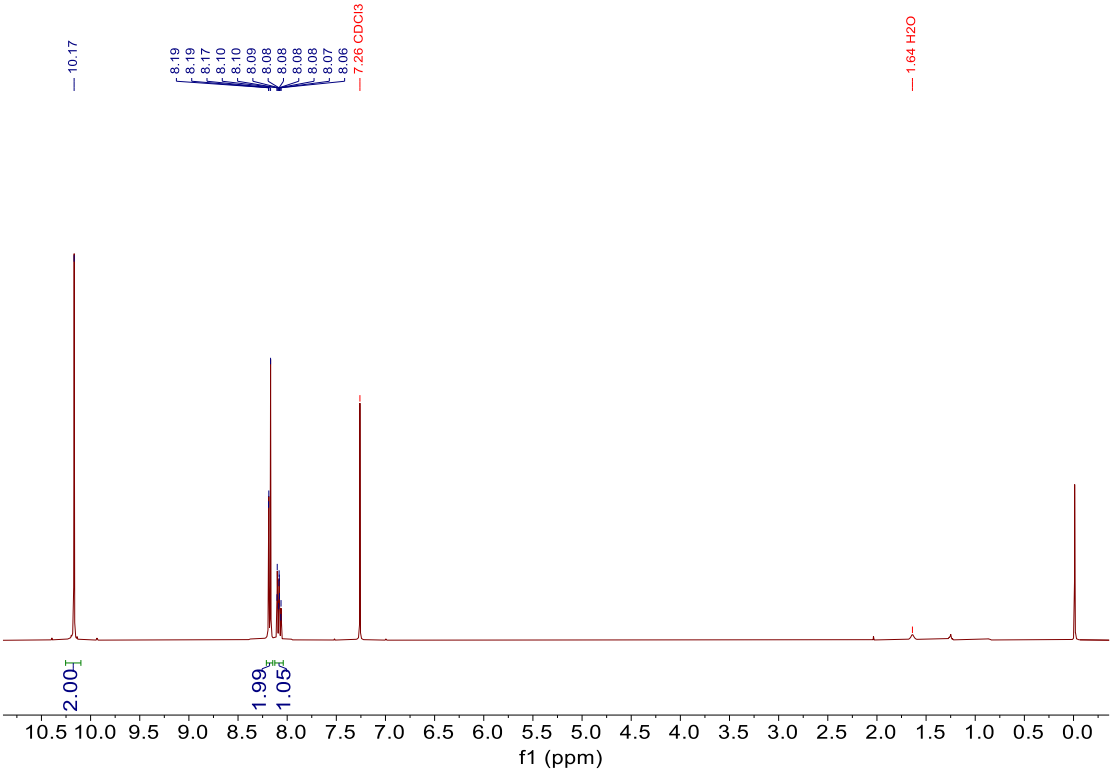

Figure S3. ^{1}H NMR spectrum of pyridine-2,6-dicarbaldehyde in $CDCl_3$.

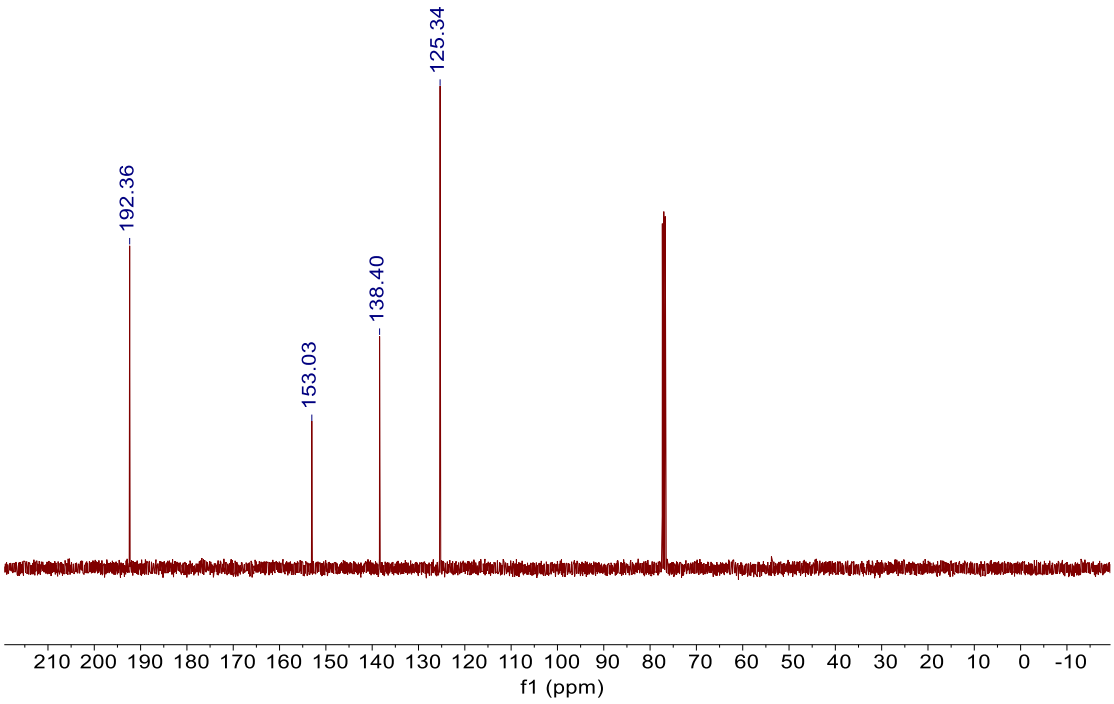

Figure S4. ^{13}C NMR spectrum of pyridine-2,6-dicarbaldehyde in $CDCl_3$.

2.2 Synthesis of 2,6-bis(isopropyliminomethyl)pyridine (L1)

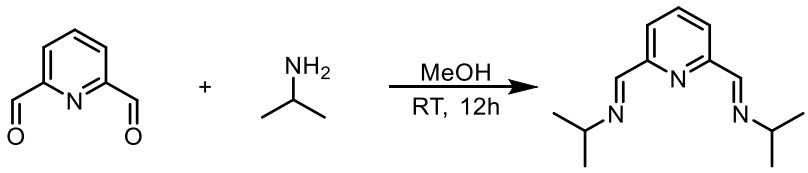

2,6-bis(isopropyliminomethyl)pyridine (**L1**) was synthesized following a previously described procedure in the literature.[S4] Isopropylamine (0.236 g, 4 mmol) was dissolved in methanol (20 mL), to which 2,6-pyridinedicarboxaldehyde (0.274 g, 2 mmol) and catalytic amounts of *p*-toluenesulfonyl chloride (2 mg, 10 μmol) were added. The mixture was refluxed for 6 hours, then filtered, and the solvent was evaporated. The remaining residue was extracted with hexane, and the reddish-brown oil of 2,6-bis(isopropyliminomethyl)pyridine (**L1**) (0.387 g, 89% yield) was obtained after the removal of hexane under vacuum. ^{1}H NMR (400 MHz, $CDCl_3$) δ 8.42 (s, 2H), 8.01 (d, J = 7.7 Hz, 2H), 7.76 (t, J = 7.8 Hz, 1H), 3.64 (hept, J = 6.3 Hz, 2H), 1.27 (d, J = 6.3 Hz, 12H). ^{13}C NMR (101 MHz, $CDCl_3$) δ 159.03, 154.54, 136.95, 122.07, 61.35, 23.93.

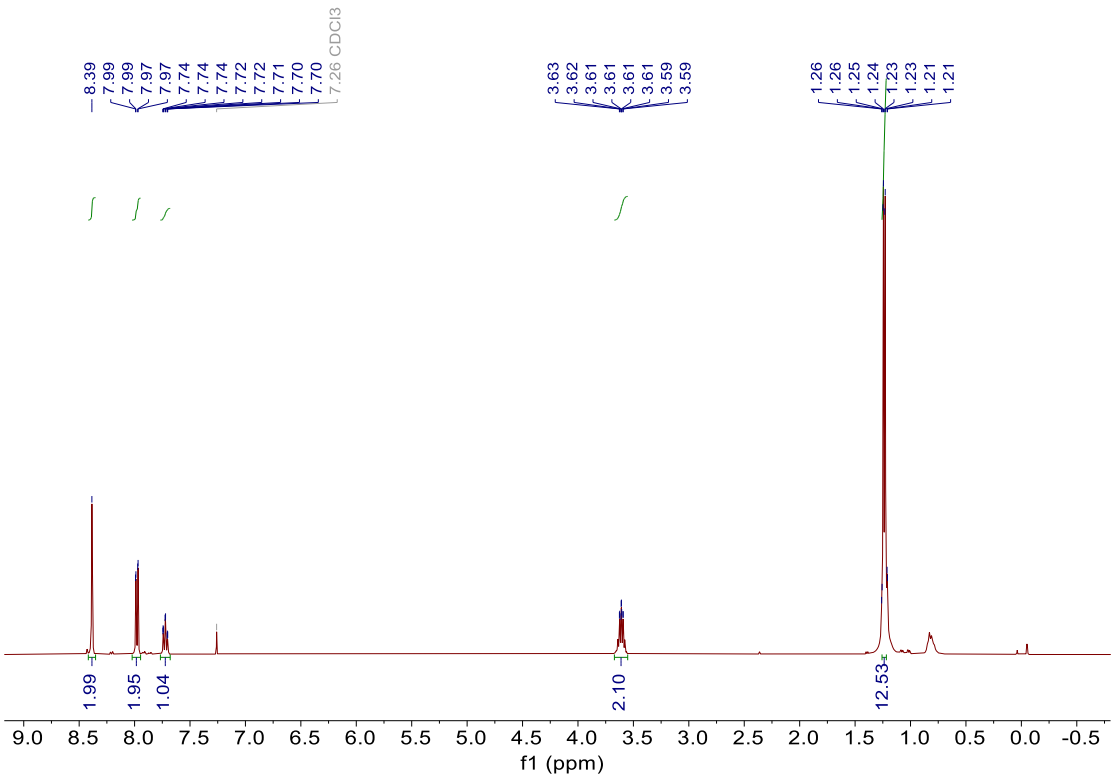

Figure S5. ^{1}H NMR spectrum of 2,6-bis(isopropyliminomethyl)pyridine **(L1).**

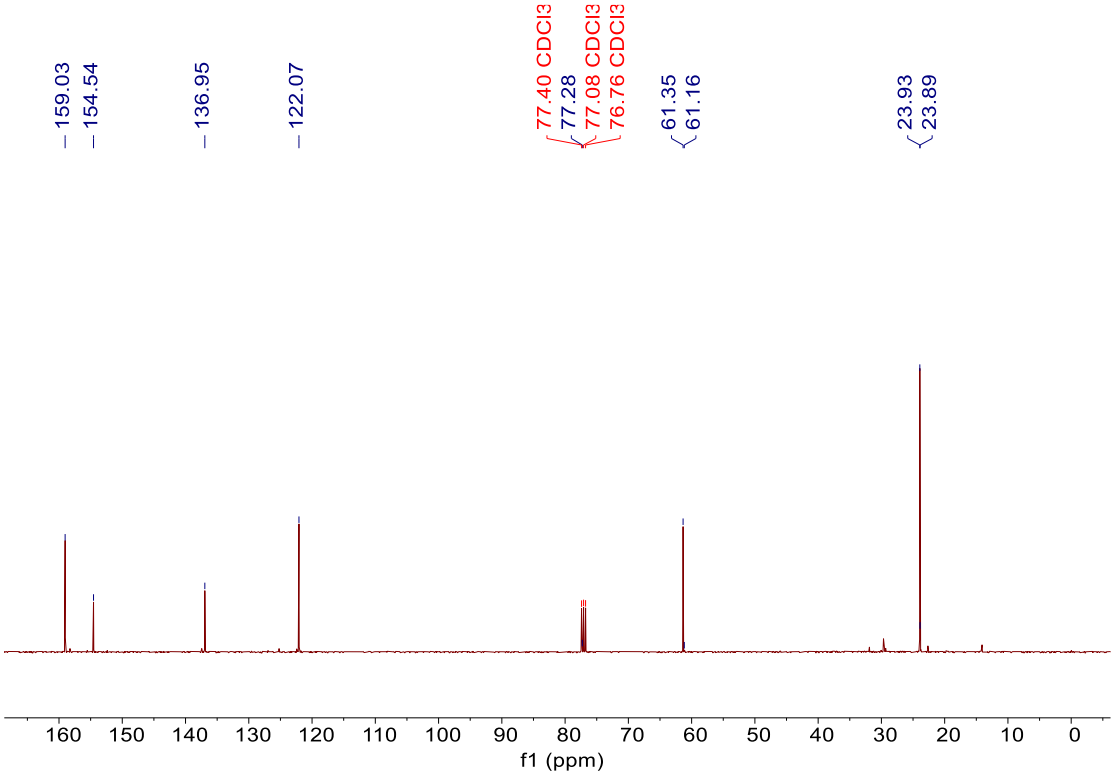

Figure S6. ^{13}C NMR spectrum of 2,6-bis(isopropyliminomethyl)pyridine **(L1)**.

2.3 Synthesis of 2,6-bis(*N*-tert-butyliminomethyl)pyridine (L2).

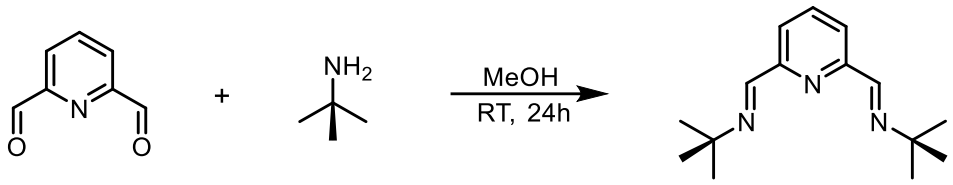

2,6-bis(*N*-tert-butyliminomethyl)pyridine (**L2**) was synthesized using a method similar to that of **L1**, with the substitution of tert-butylamine for isopropylamine.[S4] After refluxing and subsequent filtration, the residue was extracted with hexane. The reddish-brown oil of 2,6-bis(*N*-tert-butyliminomethyl)pyridine (**L2**) (0.416 g, 85% yield) was obtained following the removal of hexane under vacuum. ^{1}H NMR (400 MHz, $CDCl_3$) δ 8.39 (s, 2H), 8.04 (d, *J* = 7.7 Hz, 2H), 7.76 (t, *J* = 7.8 Hz, 1H), 1.30 (s, 18H). ^{13}C NMR (101 MHz, $CDCl_3$) δ 156.25, 155.11, 137.08, 121.69, 57.96, 29.62.

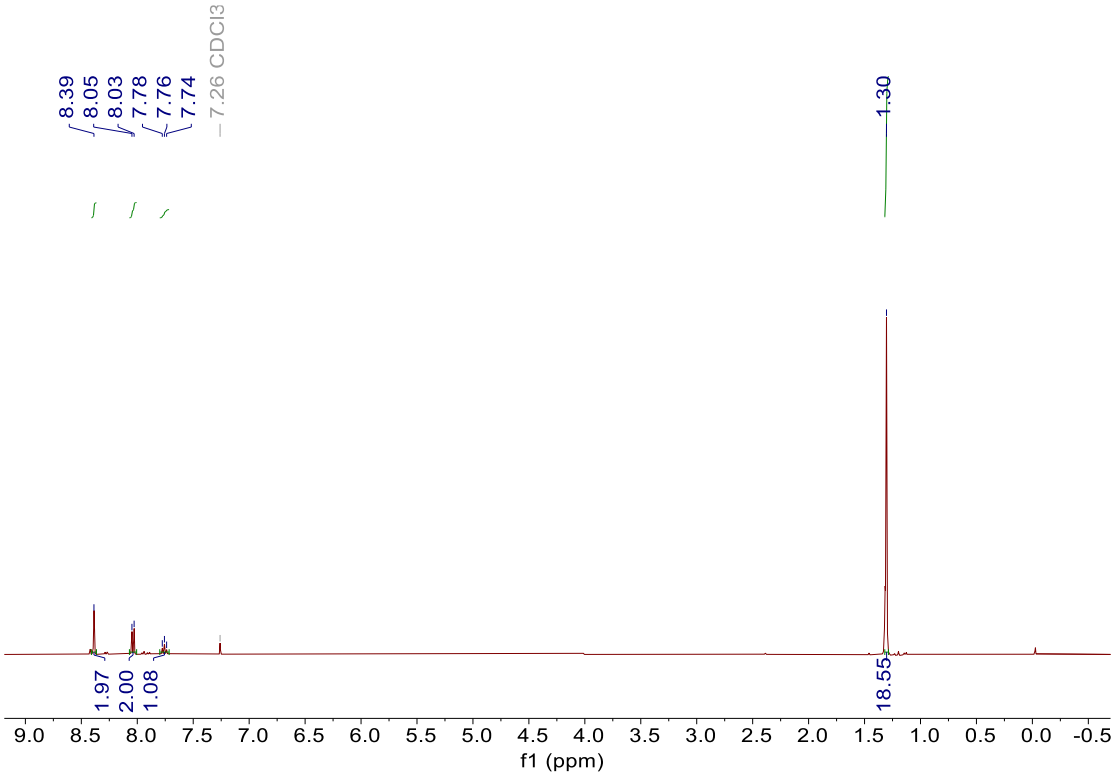

Figure S7. ^{1}H NMR spectrum of 2,6-bis(*N*-tert-butyliminomethyl)pyridine **(L2)**.

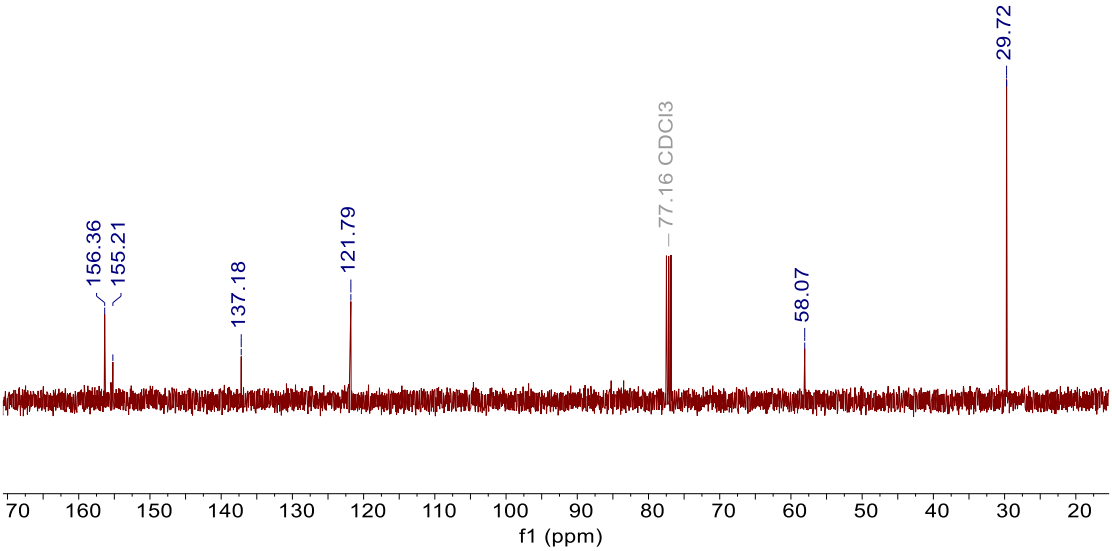

Figure S8. ^{13}C NMR spectrum of 2,6-bis(*N*-tert-butyliminomethyl)pyridine **(L2)**.

2.4 Synthesis of 2,6-bis(2,4,6-trimethylphenyliminomethyl)pyridine **(L3)**.

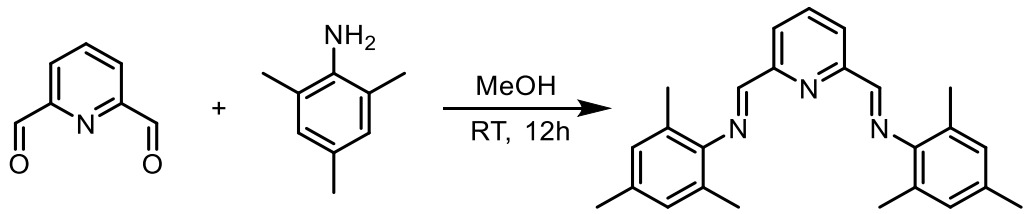

2,6-bis(2,4,6-trimethylphenyliminomethyl)pyridine (**L3**) was synthesized according to a procedure outlined in the literature.[S5] 2,4,6-trimethylaniline (0.135 g, 1 mmol) was dissolved in methanol (30 mL), to which pyridine-2,6-dicarbaldehyde (0.068 g, 0.5 mmol) and 5 drops of formic acid were added. The mixture was stirred at room temperature for 12 hours. After stirring, the solution was filtered, and the resultant golden yellow solid of 2,6-bis(2,4,6-trimethylphenyliminomethyl)pyridine (**L3**) (0.157 g, 85% yield) was obtained following washing with cold methanol and drying under vacuum. ^{1}H NMR (400 MHz, $CDCl_3$) δ 8.41 – 8.37 (m, 4H), 7.97 (t, J = 7.8 Hz, 1H), 6.92 (d, J = 1.2 Hz, 4H), 2.31 (s, 6H), 2.17 (s, 12H). ^{13}C NMR (101 MHz, $CDCl_3$) δ 163.15, 154.55, 147.82, 137.26, 133.54, 128.85, 126.81, 122.60, 77.25, 20.78, 18.28.

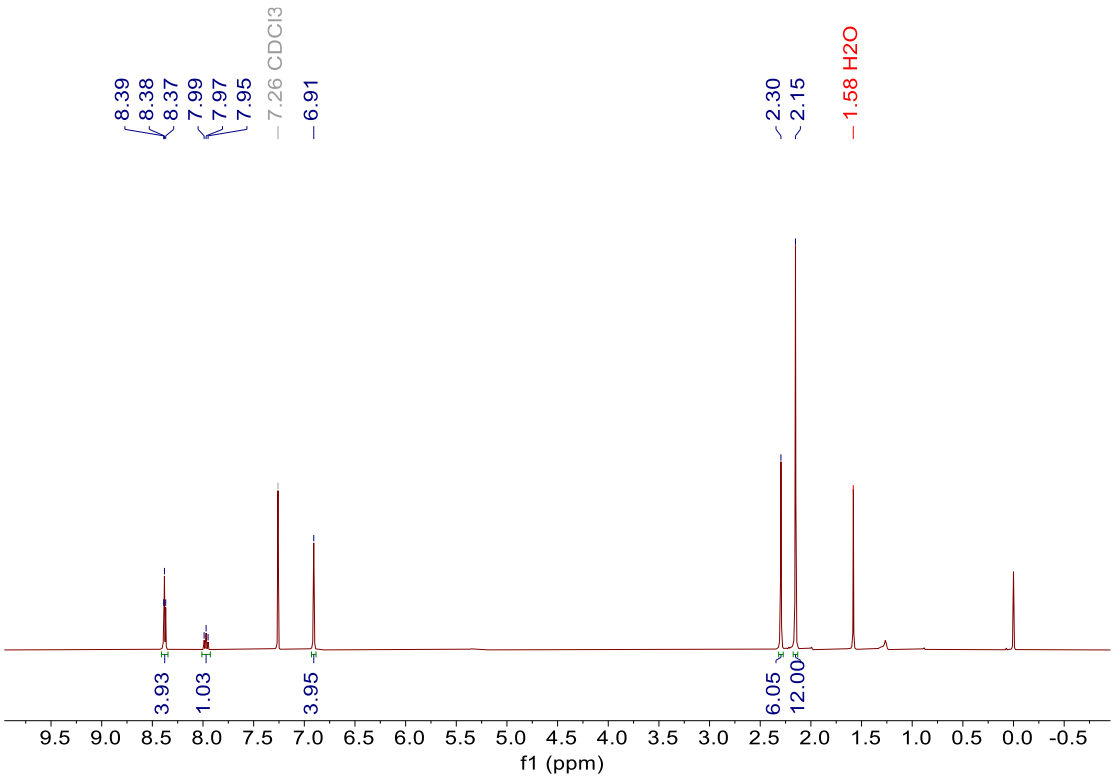

Figure S9. ^{1}H NMR spectrum of 2,6-bis(2,4,6-trimethylphenyliminomethyl)pyridine (**L3**).

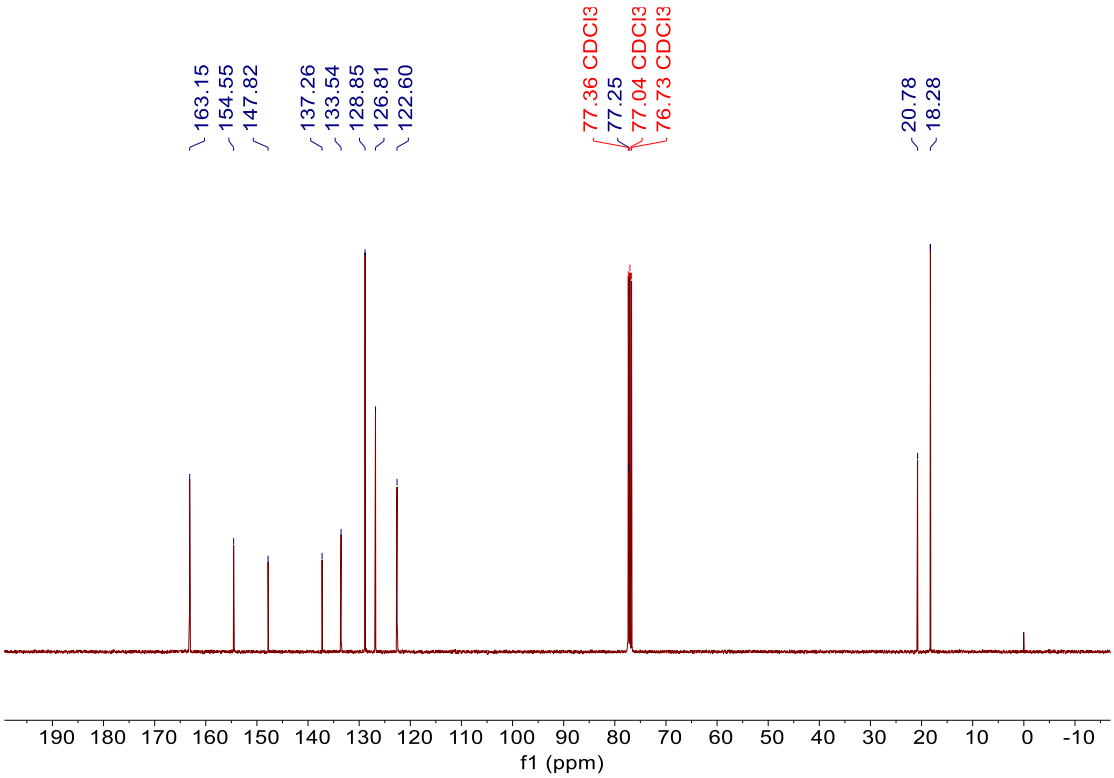

Figure S10. ^{13}C NMR spectrum of 2,6-bis(2,4,6-trimethylphenyliminomethyl)pyridine (**L3**).

2.5 Synthesis of 2,6-bis(2,6-diisopropylphenyliminomethyl)pyridine (L4).

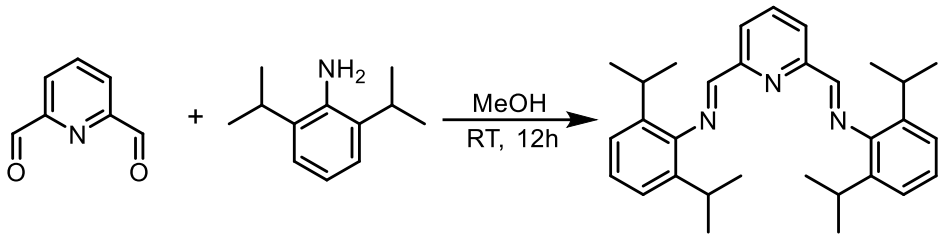

2,6-bis(2,6-diisopropylphenyliminomethyl)pyridine (**L4**) was synthesized following a method described in the literature.[S6] 2,6-diisopropylaniline (0.178 g, 1 mmol) was dissolved in methanol (30 mL), to which pyridine-2,6-dicarbaldehyde (0.068 g, 0.5 mmol) along with 5 drops of formic acid were added. The mixture was stirred at room temperature for 12 hours. Then, the solution was filtered and the resultant dark yellow solid of 2,6-bis(2,6-diisopropylphenyliminomethyl)pyridine (**L4**) (0.20 g, 88% yield) was obtained after washing with cold methanol and drying under vacuum. ^{1}H NMR (400 MHz, $CDCl_3$) δ 8.44 – 8.34 (m, 4H), 8.06 – 7.94 (m, 1H), 7.22 – 7.10 (m, 6H), 3.00 (hept, J = 6.9 Hz, 4H), 1.20 (d, J = 6.8 Hz, 24H). ^{13}C NMR (101 MHz, $CDCl_3$) δ 162.71, 154.46, 148.32, 137.37, 137.16, 124.55, 123.07, 122.77, 77.23, 28.01, 23.46.

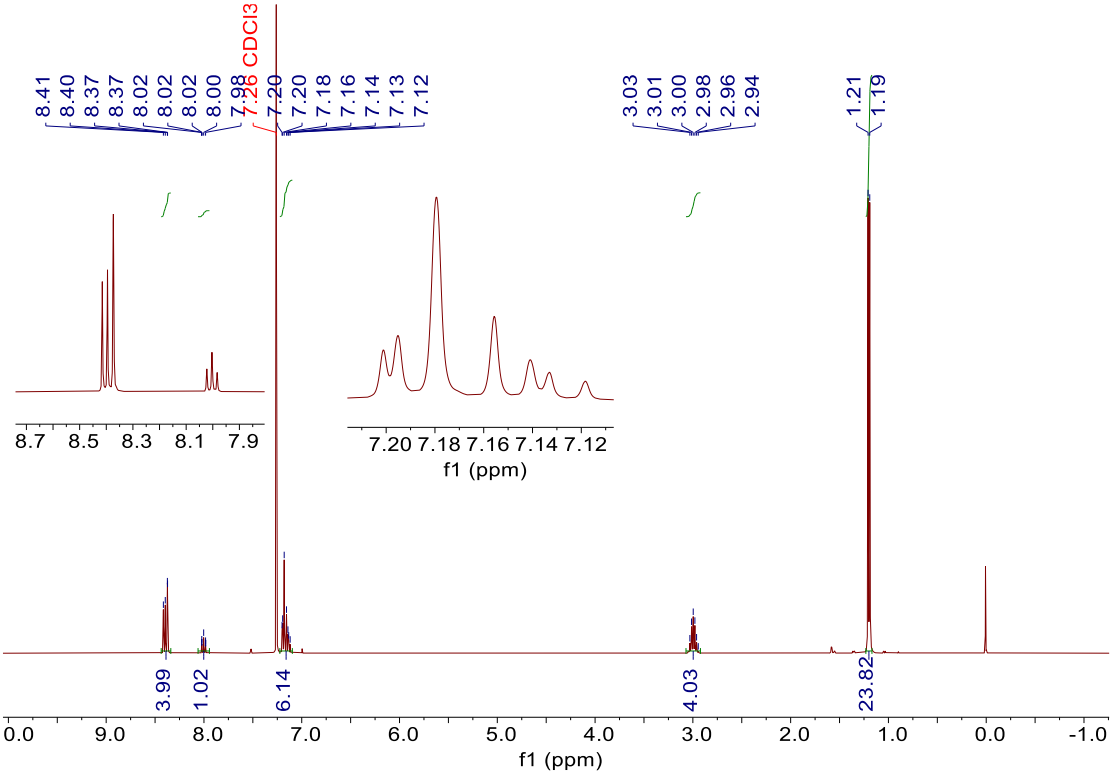

Figure S11. ^{1}H NMR spectrum of 2,6-bis(2,6-diisopropylphenyliminomethyl)pyridine (**L4**).

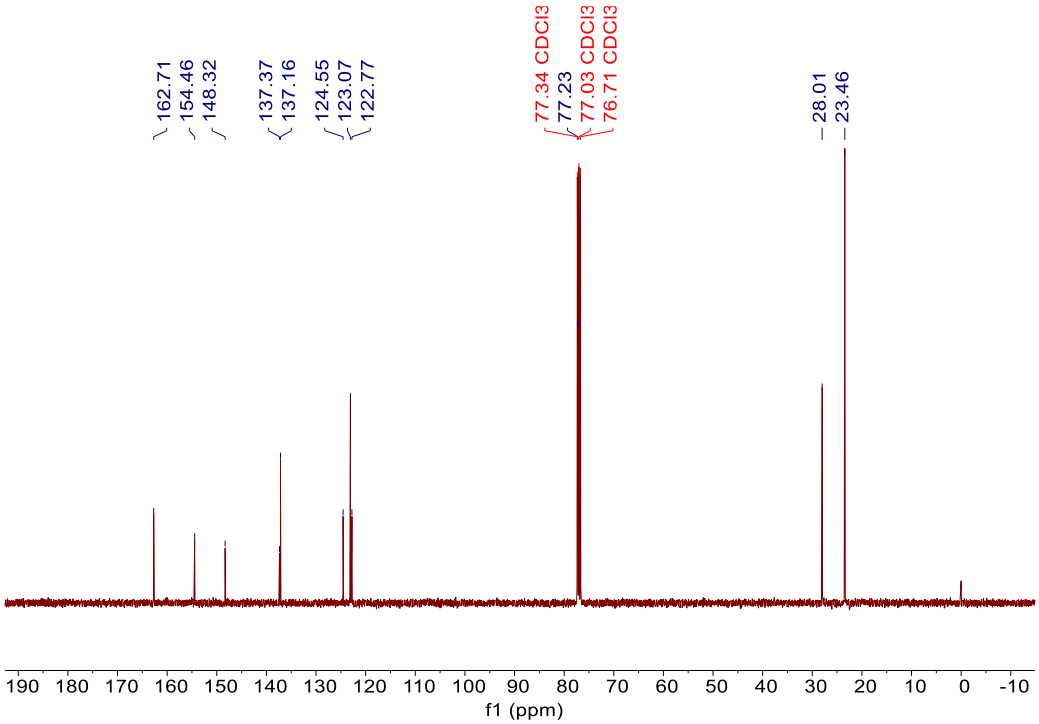

Figure S12. ^{13}C NMR spectrum of 2,6-bis(2,6-diisopropylphenyliminomethyl)pyridine (**L4**).

2.6 Synthesis of [Ru(L1)Cl$_2$(PPh$_3$)] (C1).

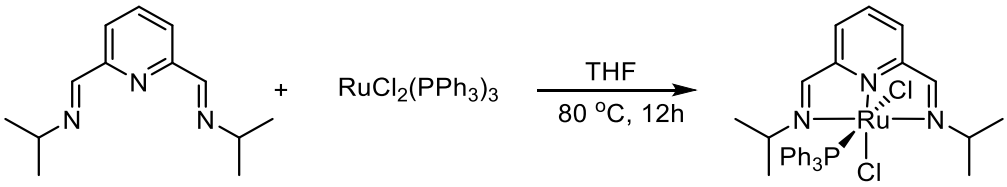

[Ru(**L1**)Cl$_2$(PPh$_3$)] (**C1**) was synthesized according to a procedure described in previous literature.[S4] 2,6-bis(isopropyliminomethyl)pyridine (**L1**) (0.0868 g, 0.4 mmol) and RuCl$_2$(PPh$_3$)$_3$ (0.2874 g, 0.3 mmol) were dissolved in anhydrous THF (20 mL) under an argon atmosphere. The mixture was refluxed for 12 hours, during which the color changed from violet to reddish-brown. Afterwards, the solvent was removed, and the residue was washed with diethyl ether (3×10 mL) and pentane (3×10 mL). The reddish-brown solid of [Ru(**L1**)Cl$_2$(PPh$_3$)] (**C1**) (0.156 g, 80% yield) was obtained after vacuum drying. Crystals suitable for X-ray analysis were produced by slowly diffusing pentane (4 mL) into a dichloromethane solution (2 mL) of **C1** (20 mg). Anal. Calc. for $C_{31}H_{34}Cl_2N_3PRu{\cdot}CH_2Cl_2$: C, 52.19; H, 4.93; N, 5.71. Found: C, 52.24; H, 5.01; N, 5.76.

^{1}H NMR (400 MHz, $CDCl_3$) δ 7.99 (s, 2H), 7.72−7.62 (m, 6H), 7.25−7.09 (m, 12H), 4.81 (p, J = 6.6 Hz, 2H), 1.58 (d, 6H), 0.87 (d, 6H). ^{31}P NMR (162 MHz, $CDCl_3$) δ 29.15. ^{13}C NMR (101 MHz, $CDCl_3$) δ 162.22, 160.54, 132.59, 132.49, 131.98, 129.20, 128.28, 128.05, 127.96, 123.02, 77.25, 59.19, 25.44, 21.54.

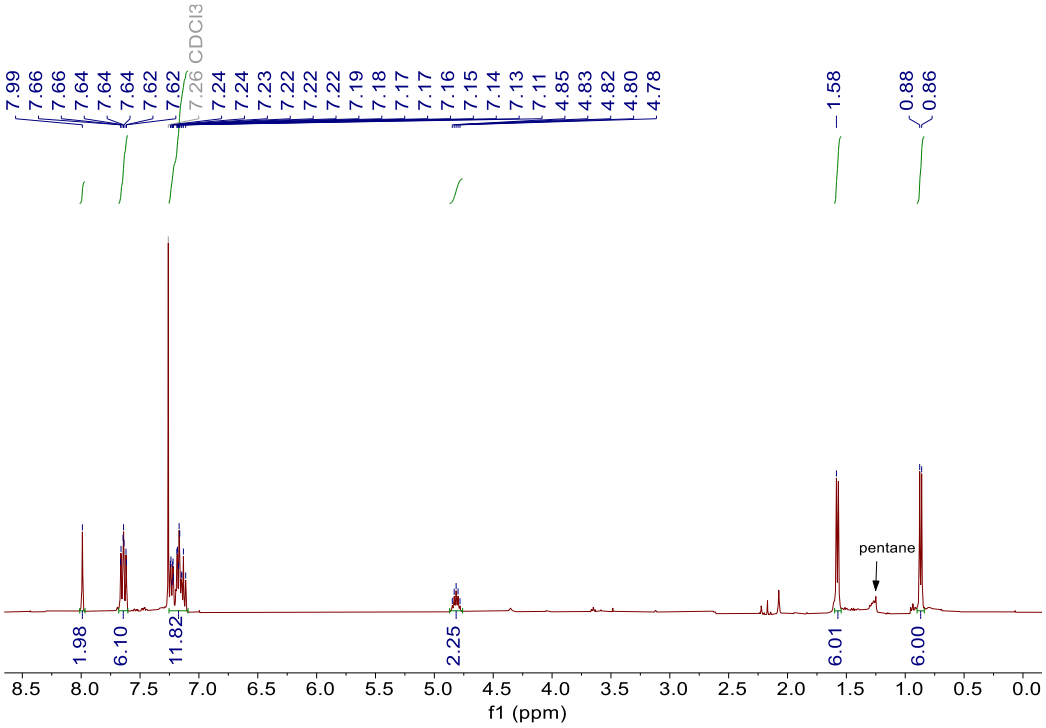

Figure S13. ^{1}H NMR spectrum [Ru(**L1**)Cl_2(PPh_3)] (**C1**).

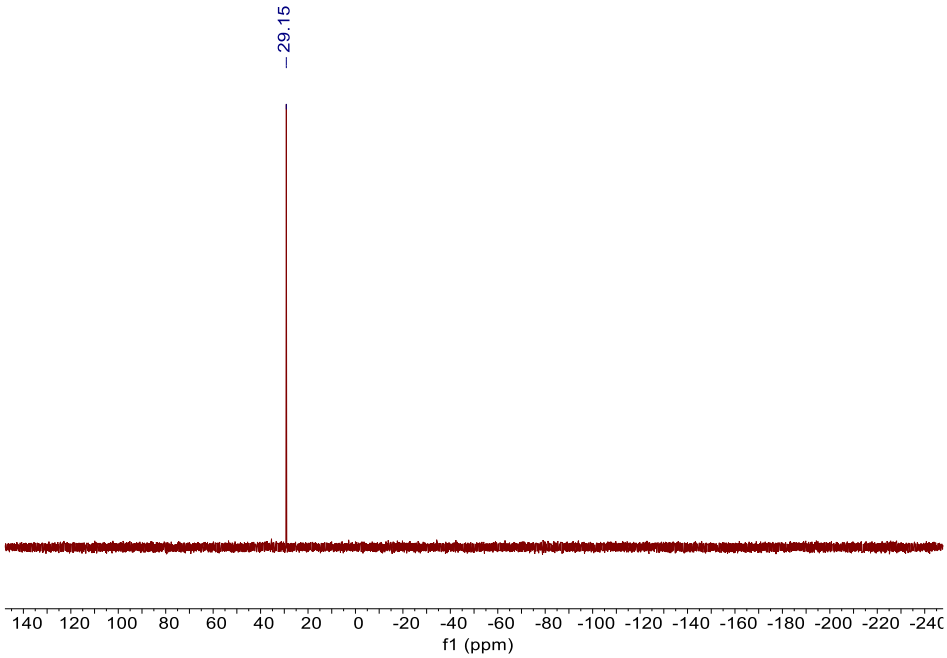

Figure S14. ^{31}P NMR spectrum [Ru(**L1**)Cl_2(PPh_3)] (**C1**).

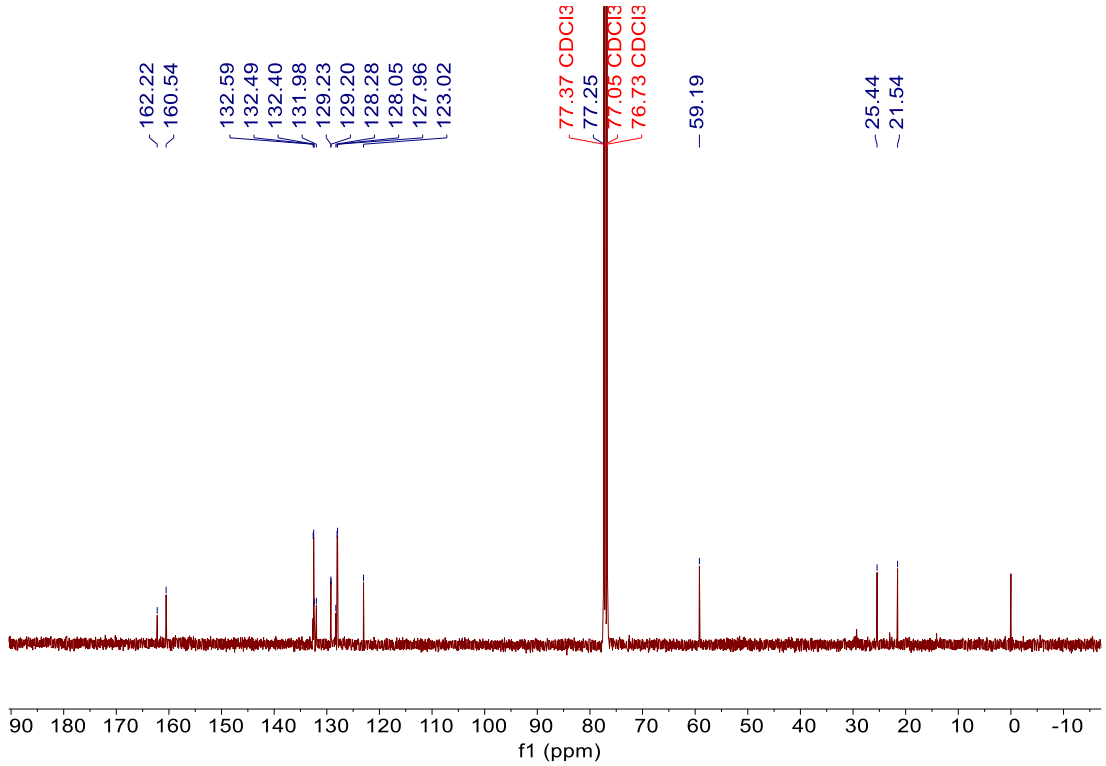

Figure S15. ^{13}C NMR spectrum [Ru(**L1**)Cl_2(PPh_3)] (**C1**).

2.7 Synthesis of [Ru(L2)Cl_2(PPh_3)] (C2).

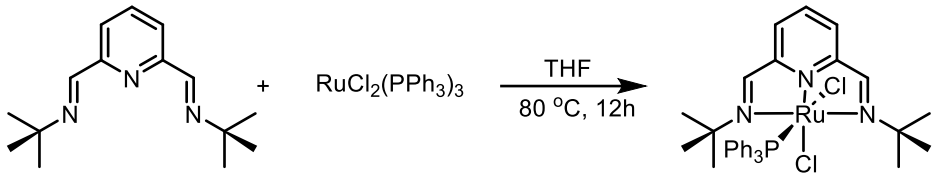

[Ru(**L2**)Cl_2(PPh_3)] **(C2)** was synthesized following a method described in previous literature.[S6] 2,6-bis(*N*-tert-butyliminomethyl)pyridine (**L2**) (0.098 g, 0.4 mmol) and $RuCl_2(PPh_3)_3$ (0.2874 g, 0.3 mmol) were dissolved in anhydrous THF (20 mL) under an argon atmosphere. The mixture was refluxed for 12 hours, during which the color transitioned from violet to reddish-brown. After the reaction, the solvent was removed, and the residue was washed sequentially with diethyl ether (3×10 mL) and pentane (3×10 mL). The reddish-brown solid of [Ru(**L2**)Cl_2(PPh_3)] **(C2)** (0.152 g, 78% yield) was obtained following vacuum drying. Anal. Calc. for $C_{33}H_{38}Cl_2N_3PRu{\cdot}C_5H_{12}$: C, 60.71; H, 6.70; N, 5.59. Found: C, 60.82; H, 6.75; N, 5.64. ^{1}H NMR (400 MHz, $CDCl_3$) δ 7.93 (s, 1H), 7.80 (s, 1H), 7.76 – 7.29 (m, 6H), 7.21 – 6.89 (m, 10H), 6.71 (d, J = 7.6 Hz, 2H), 2.70 (dq, J = 14.9, 7.4 Hz, 2H), 2.17 (dq, J = 15.1, 7.5 Hz, 2H), 1.68 (s, 6H),

0.91 (t, J = 7.5 Hz, 8H). ^{31}P NMR (162 MHz, $CDCl_3$) δ 23.84. ^{13}C NMR (101 MHz, $CDCl_3$) δ 171.02, 159.26, 152.31, 137.34, 134.97, 134.87, 134.67, 134.31, 132.81, 132.29, 132.19, 128.72, 128.57, 127.12, 126.78, 126.69, 126.61, 25.38, 22.47, 15.27, 14.20.

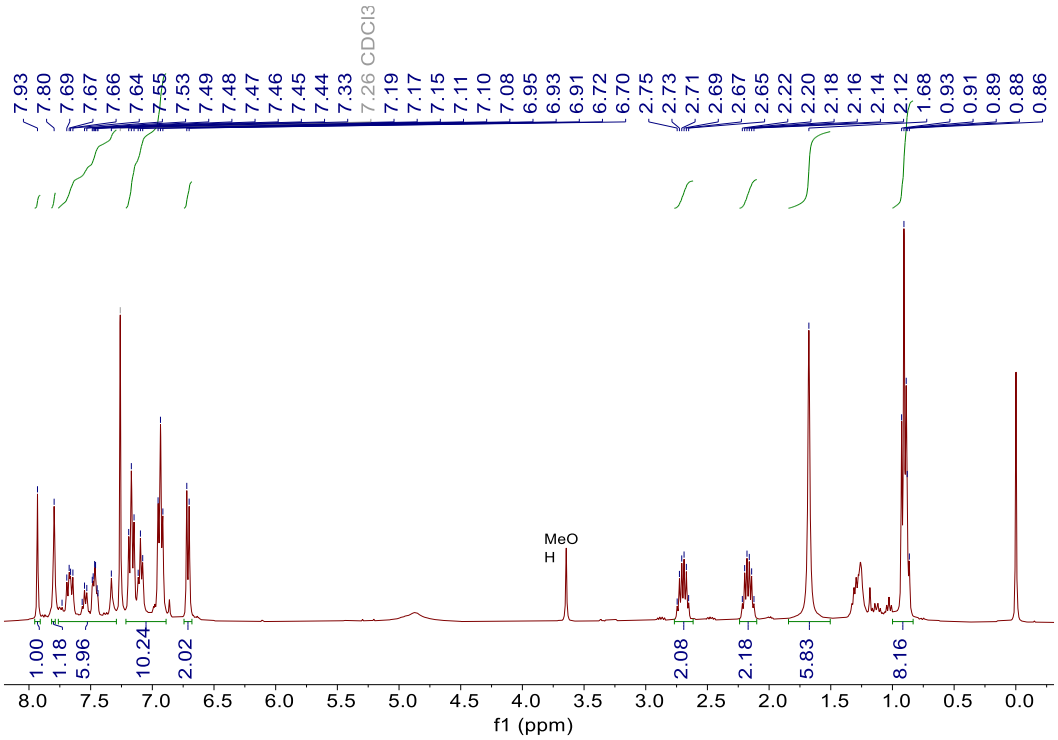

Figure S16. ^{1}H NMR spectrum [Ru(**L2**)Cl_2(PPh_3)] (**C2**).

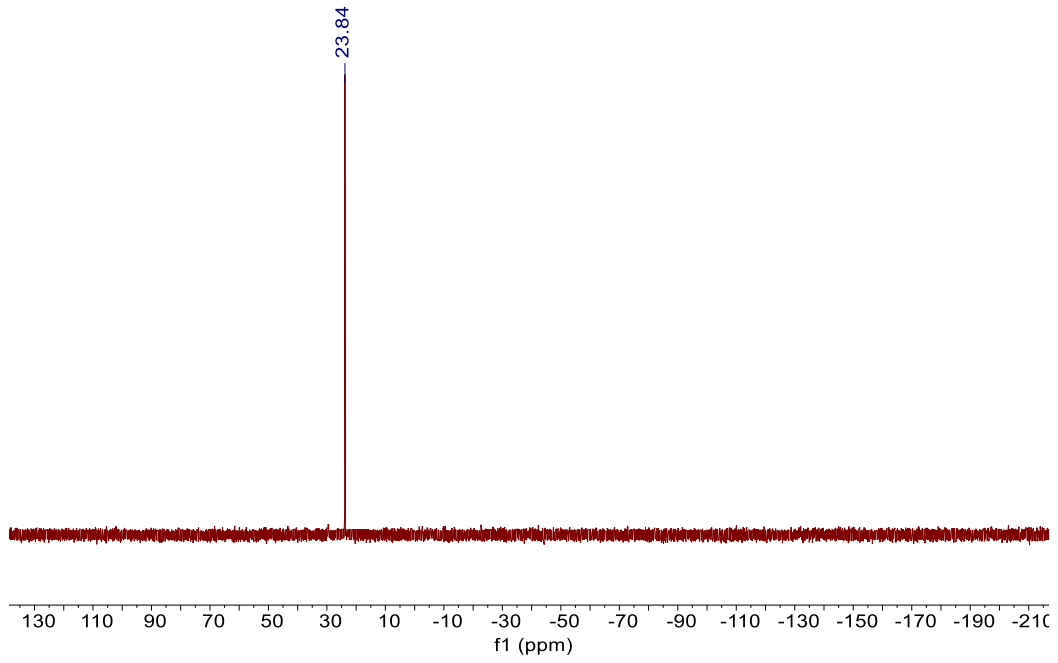

Figure S17. ^{31}P NMR spectrum [Ru(**L2**)Cl_2(PPh_3)] (**C2**).

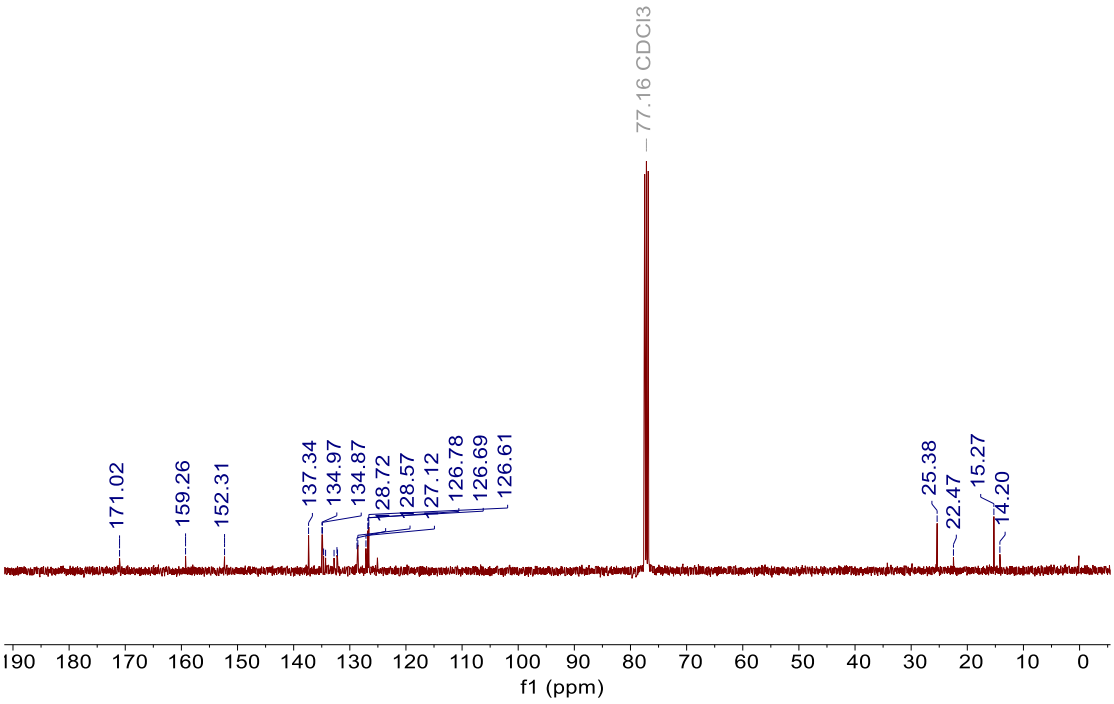

Figure S18. ^{13}C NMR spectrum [Ru(**L2**)Cl_2(PPh_3)] (**C2**).

2.8 Synthesis of [Ru(L3)Cl_2(PPh_3)] (C3).

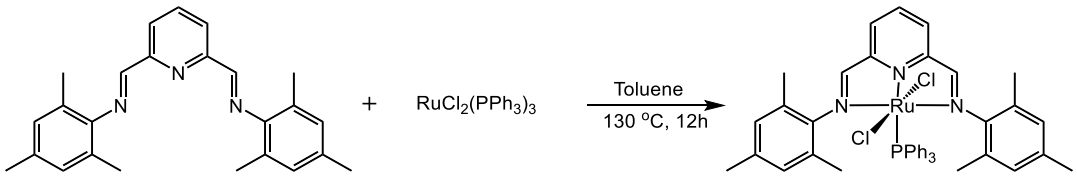

2,6-bis(2,4,6-trimethylphenyliminomethyl)pyridine (**L3**) (0.1107 g, 0.3 mmol) and $RuCl_2(PPh_3)_3$ (0.2874 g, 0.3 mmol) were dissolved in anhydrous toluene (20 mL) under an argon atmosphere. The mixture was refluxed for 12 hours, during which the color remained dark violet. Then, the solvent was removed, and the residue was washed with diethyl ether (3×10mL) followed by pentane (3×10 mL). A small amount of dichloromethane (5 mL) was added to dissolve the residue completely, then pentane (30 mL) was added dropwise under stirring. After filtering the solution, the dark violet solid of[Ru(**L3**)Cl_2(PPh_3)] (**C3**) (0.157 g, 65% yield) was obtained following vacuum drying. Crystals suitable for X-ray analysis were produced by slow evaporation of a methanol solution (10 mL) containing 20 mg of **C3**. Anal. Calc. for $C_{43}H_{42}Cl_2N_3PRu{\cdot}CH_3OH$: C, 63.23; H, 5.55; N, 5.03. Found: C, 63.30; H, 5.62; N, 5.11.

^{1}H NMR (400 MHz, $CDCl_3$) δ 7.95 (s, 2H), 7.82−7.75 (m, 4H), 7.28−7.24 (m, 5H), 7.19–7.14 (m, 3H), 7.02–6.96 (m, 6H), 6.45 (s, 4H), 2.15 (s, 6H), 1.97 (s, 12H). ^{31}P NMR (162 MHz, $CDCl_3$) δ 23.73. ^{13}C NMR (101 MHz, $CDCl_3$) δ 170.79, 170.76, 159.51, 151.35, 135.80, 135.07, 135.04, 134.94, 134.72, 133.97, 133.78, 132.70, 131.19, 129.34, 128.18, 128.16, 126.71, 126.62, 124.83, 124.81, 20.78, 20.61, 20.54. HRMS (ESI): *m/z* calculated for $[C_{43}H_{42}Cl_2N_3PRu-Cl]^+$: 768.1848; Found: 768.1847.

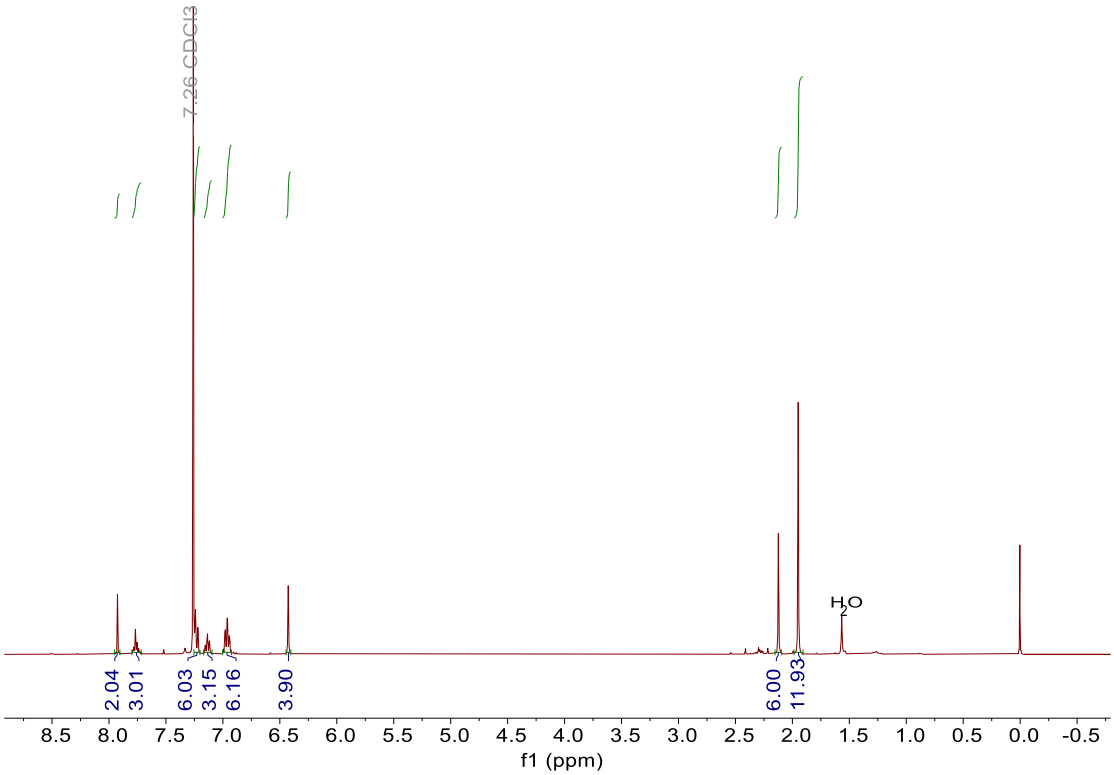

Figure S19. ^{1}H NMR spectrum [Ru(**L3**)Cl_2(PPh_3)] (**C3**).

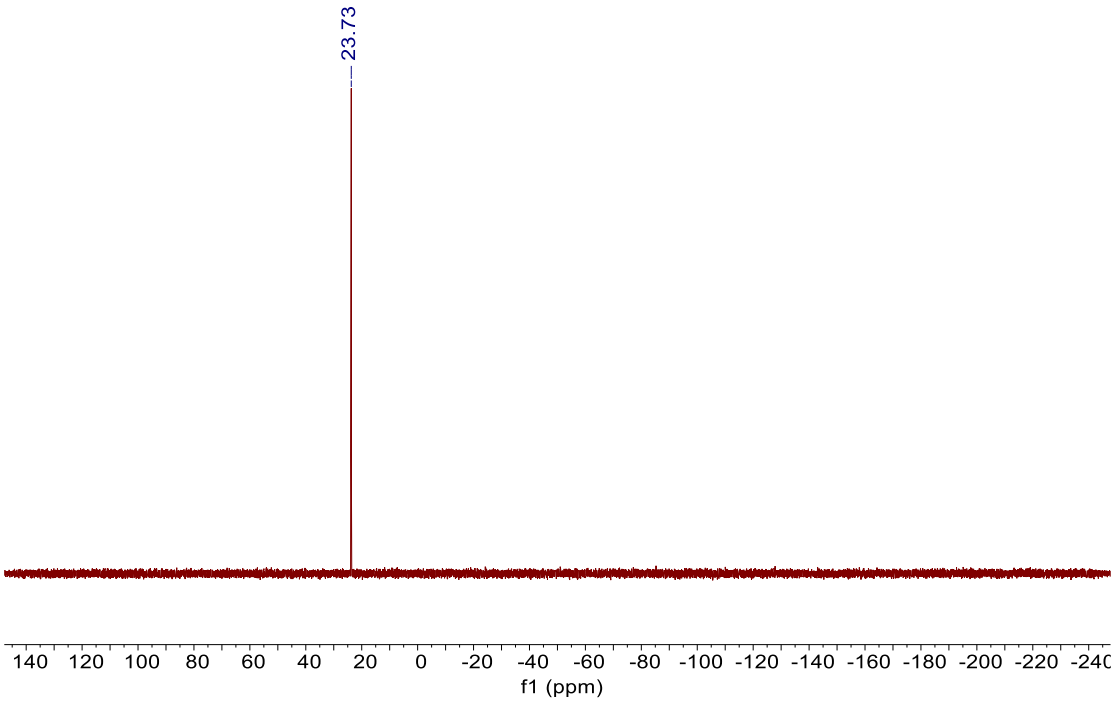

Figure S20. ^{31}P NMR spectrum [Ru(**L3**)Cl_2(PPh_3)] (**C3**).

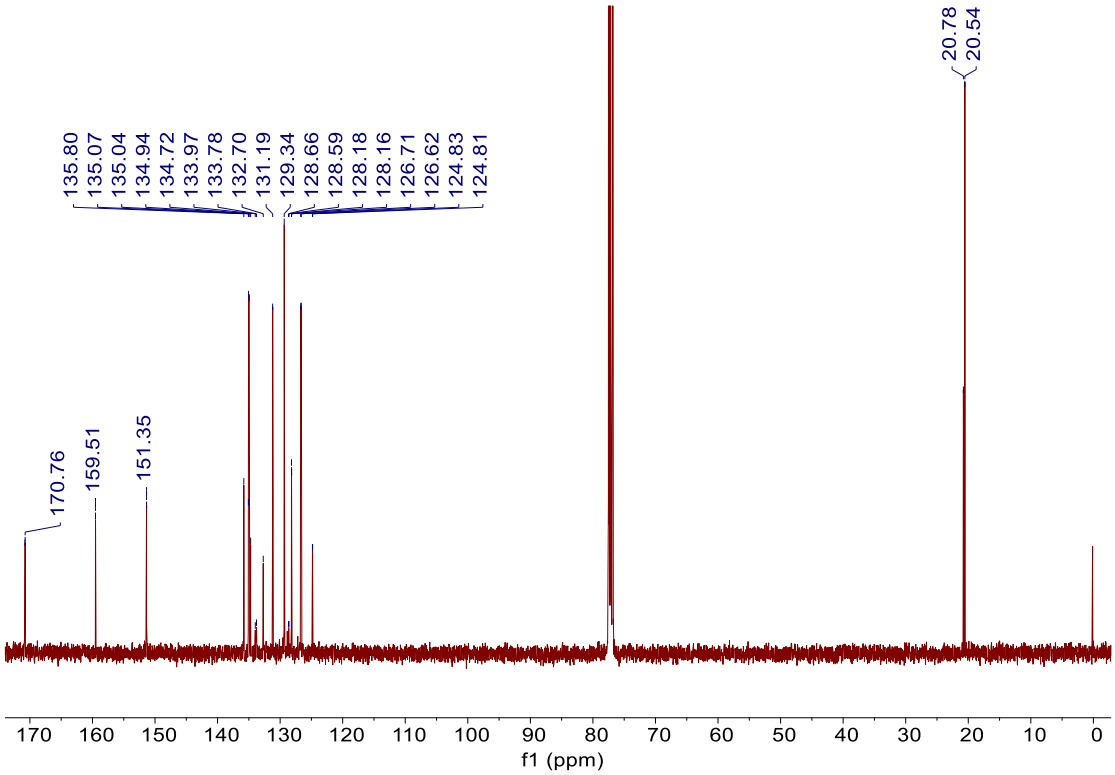

Figure S21. ^{13}C NMR spectrum [Ru(**L3**)Cl_2(PPh_3)] (**C3**).

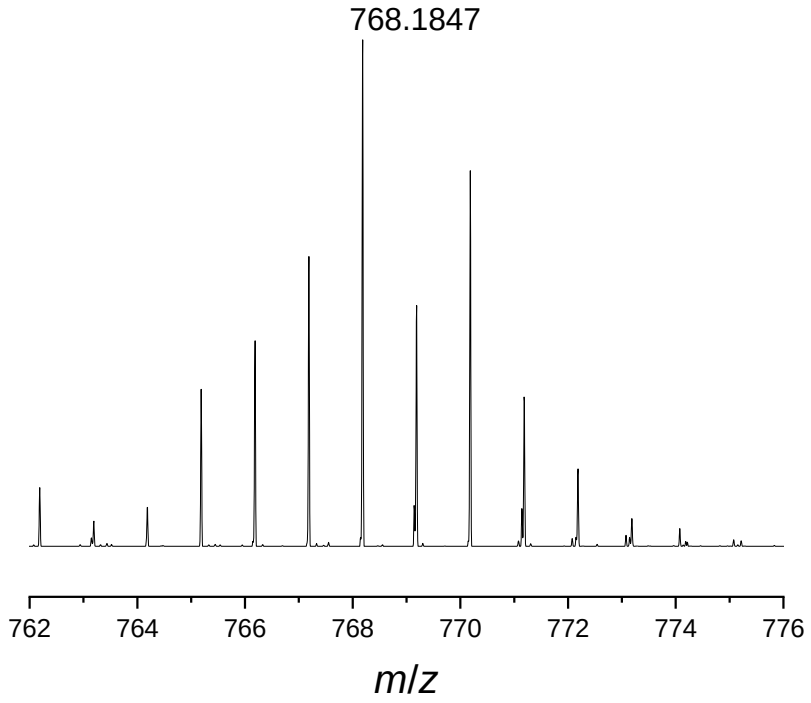

Figure S22. HRESI-MS data of **C3**.

2.9 Synthesis of [Ru(L4)Cl_2(PPh_3)] (C4).

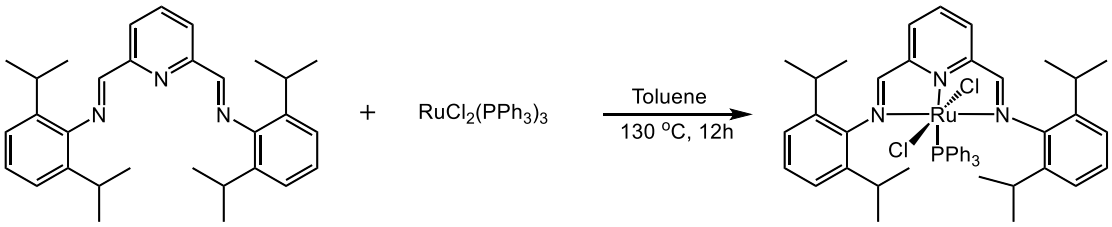

2,6-bis(2,6-diisopropylphenyliminomethyl)pyridine (**L4**) (0.1361 g, 0.3 mmol) and $RuCl_2(PPh_3)_3$ (0.2874 g, 0.3 mmol) were dissolved in anhydrous toluene (20 mL) under an argon atmosphere. The mixture was refluxed for 12 hours, during which the color remained dark violet. After this period, the solvent was evacuated, and the residue was washed with diethyl ether (3×10 mL) followed by pentane (3×10 mL). A small amount of dichloromethane (5 mL) was then added to completely dissolve the residue, after which pentane (30 mL) was added dropwise with stirring. The solution was filtered,

and the dark-violet solid of [Ru(**L4**)Cl_2(PPh_3)] (**C4**) (0.161 g, 60% yield) was obtained after vacuum drying. Crystals suitable for X-ray analysis were produced by slowly diffusing pentane (4 mL) into a dichloromethane solution (2 mL) of **C4** (20 mg). Anal. Calc. for $C_{49}H_{54}Cl_2N_3PRu{\cdot}CH_2Cl_2$: C, 61.73; H, 5.80; N, 4.32. Found: C, 61.59; H, 5.63; N, 4.42. ^{1}H NMR (400 MHz, Acetone-d6) δ 8.66 (s, 1H), 8.26 (dd, *J* = 7.8, 1.2 Hz, 1H), 8.23 (s, 1H), 8.15 (d, *J* = 7.9 Hz, 1H), 8.02 (t, *J* = 7.8 Hz, 1H), 7.45 – 7.36 (m, 4H), 7.35 – 7.23 (m, 7H), 7.22 – 7.17 (m, 2H), 7.11 (t, *J* = 7.7 Hz, 3H), 6.95 – 6.82 (m, 6H), 3.76 (hept, *J* = 6.7 Hz, 2H), 3.51 (hept, *J* = 6.7 Hz, 2H), 1.11 (d, *J* = 6.6 Hz, 7H), 1.01 (d, *J* = 6.8 Hz, 6H), 0.86 (d, *J* = 6.7 Hz, 7H), 0.61 (d, *J* = 6.7 Hz, 6H). ^{31}P NMR (162 MHz, $CDCl_3$) *δ* 16.69. ^{13}C NMR (101 MHz, $CDCl_3$) δ 171.27, 159.51, 151.67, 142.14, 134.95, 134.86, 134.15, 133.82, 132.68, 128.47, 128.27, 127.41, 127.04, 126.95, 125.03, 125.00, 123.87, 70.64, 27.59, 26.53, 25.97, 22.12. HRMS (ESI): *m/z* calculated for $[C_{49}H_{54}Cl_2N_3PRu]^{+\cdot}$: 887.2478; Found: 887.2466.

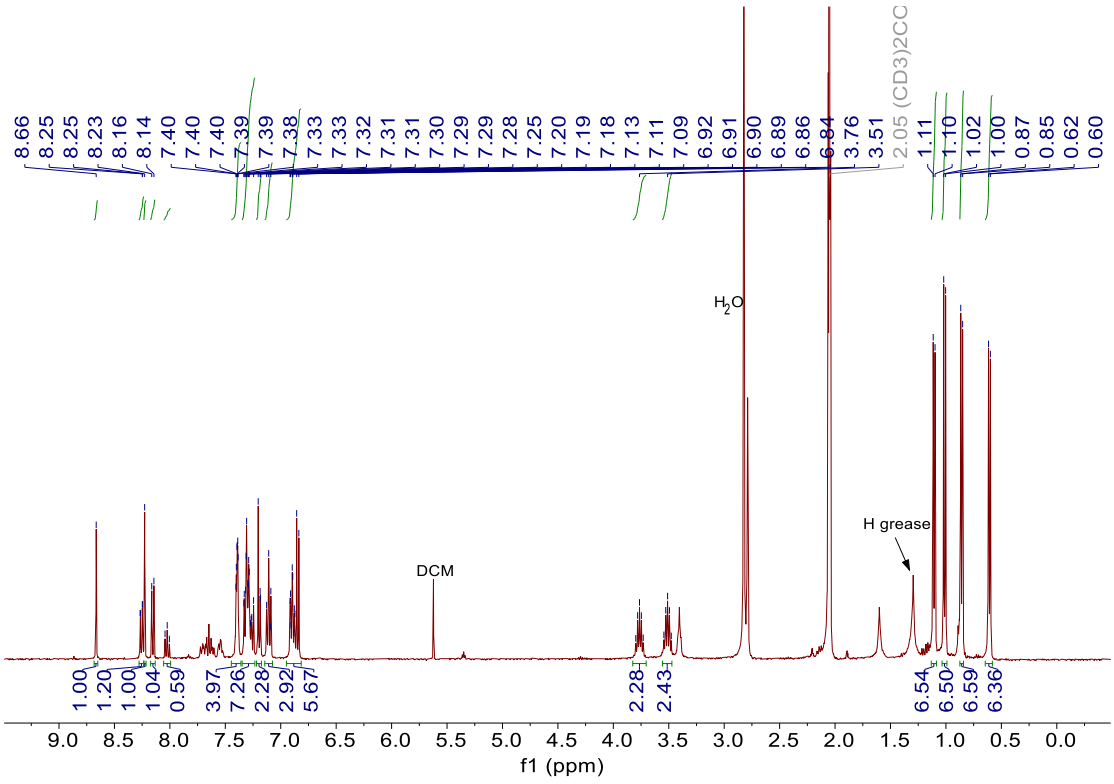

Figure S23. ^{1}H NMR spectrum [Ru(**L4**)Cl_2(PPh_3)] (**C4**) in acetone-d6.

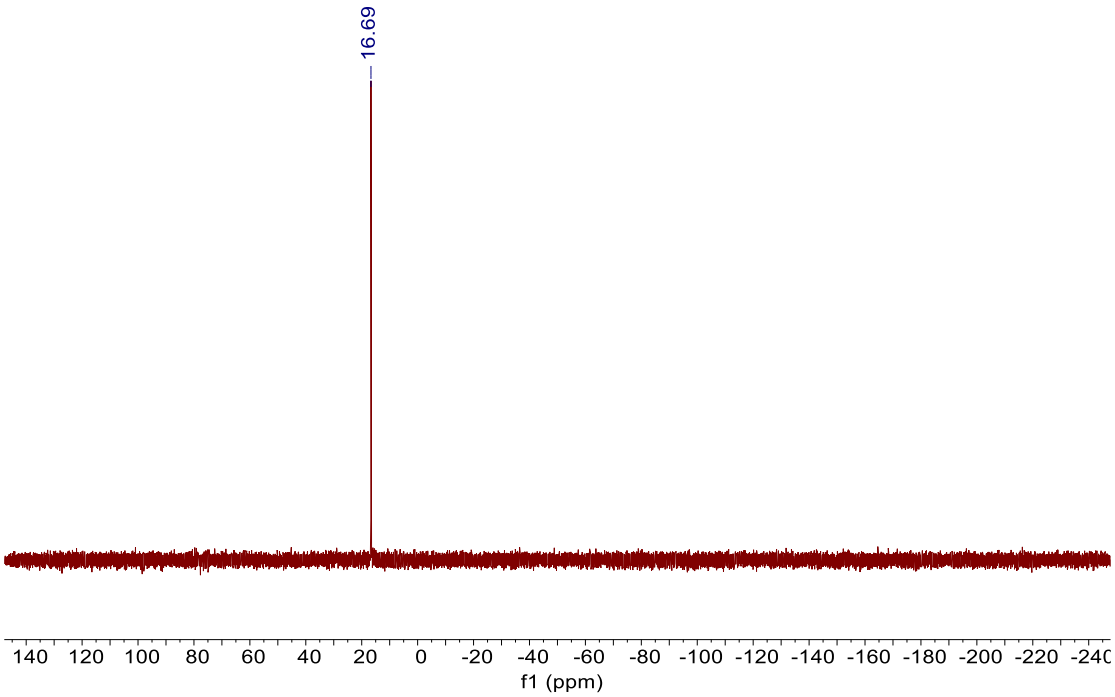

Figure S24. ^{31}P NMR spectrum [Ru(**L4**)Cl_2(PPh_3)] (**C4**) in $CDCl_3$.

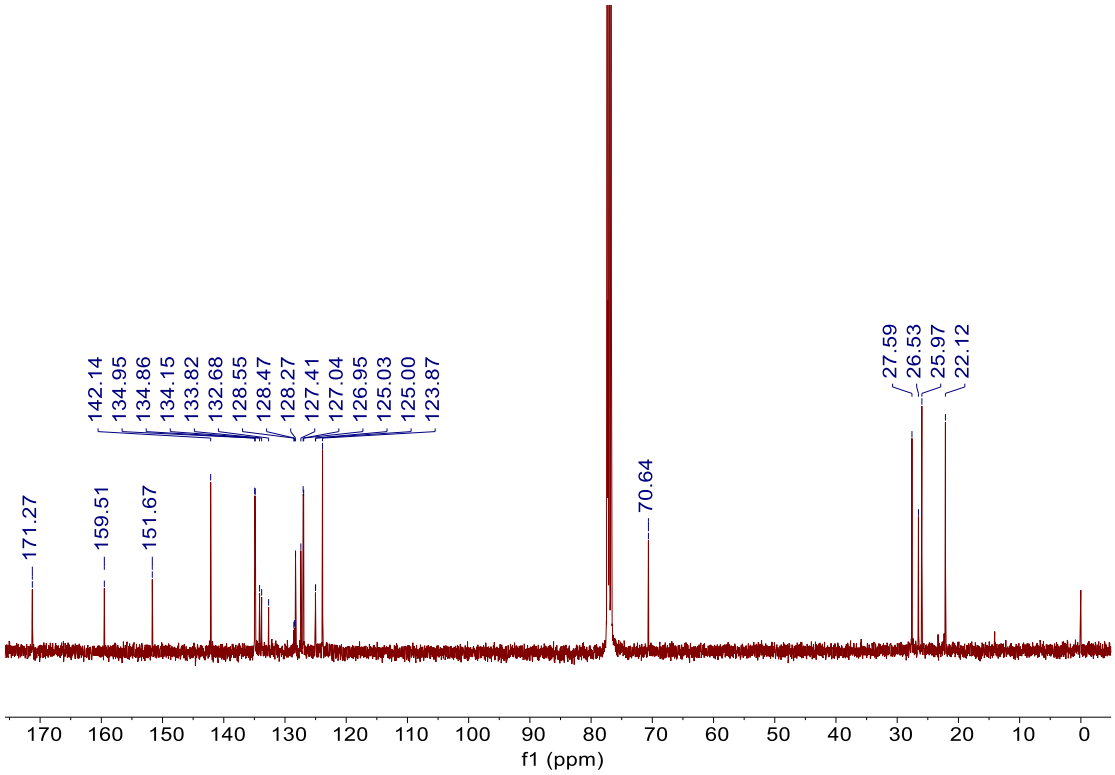

Figure S25. ^{13}C NMR spectrum [Ru(**L4**)Cl_2(PPh_3)] (**C4**) in $CDCl_3$.

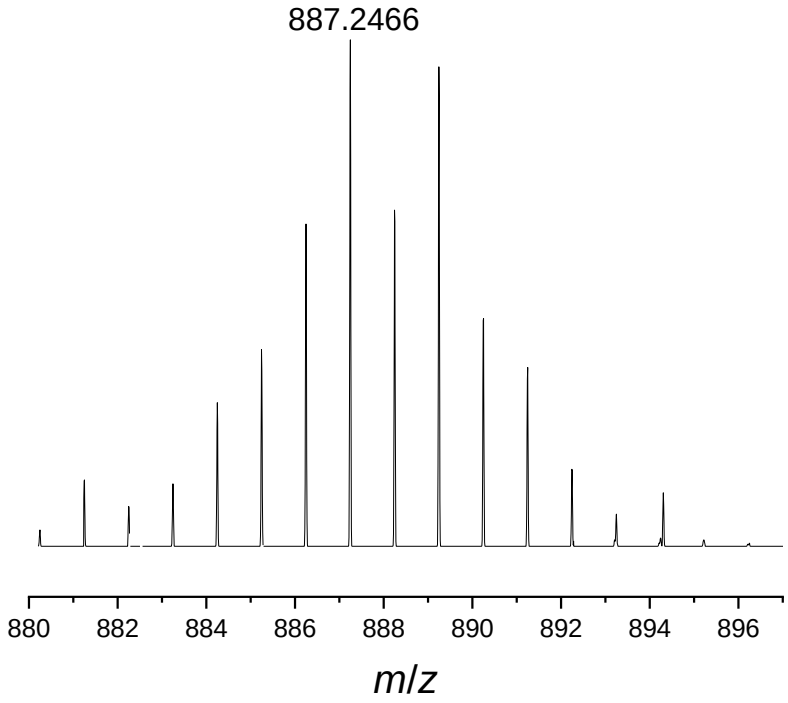

Figure S26. HRESI-MS data of **C4**.

3. Catalytic experimental data

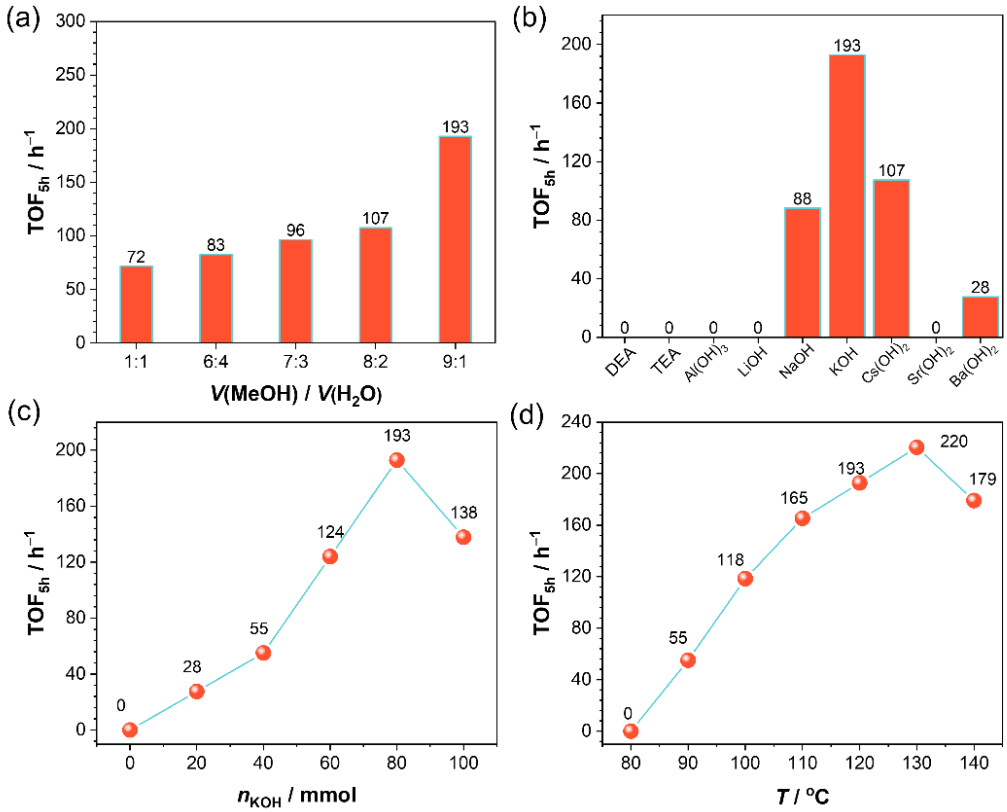

Figure S27. Optimization of reaction conditions for APRM using **C4**. a) Screening of MeOH/H_2O volumetric ratio for APRM using **C4**. Reaction conditions: MeOH/H_2O (10 mL), n_{KOH} = 80 mmol, T_{set} = 120 °C, n_{cat} = 3 μmol; b) Screening of base type on the catalytic performance using **C4**. Reaction conditions: MeOH/H_2O (v/v = 9:1, 10 mL), n_{base} = 80 mmol, T_{set} = 120 °C, n_{cat} = 3 μmol. c) Screening of KOH amount on APRM using **C4**. Reaction conditions: MeOH/H_2O (v/v = 9:1, 10 mL), T_{set} = 120 °C, n_{cat} = 3 μmol. d) Screening of reaction temperature for APRM using **C4**. Reaction conditions: MeOH/H_2O (v/v = 9:1, 10 mL), n_{KOH} = 80 mmol, n_{cat} = 3 μmol.

4. Catalytic mechanism analysis.

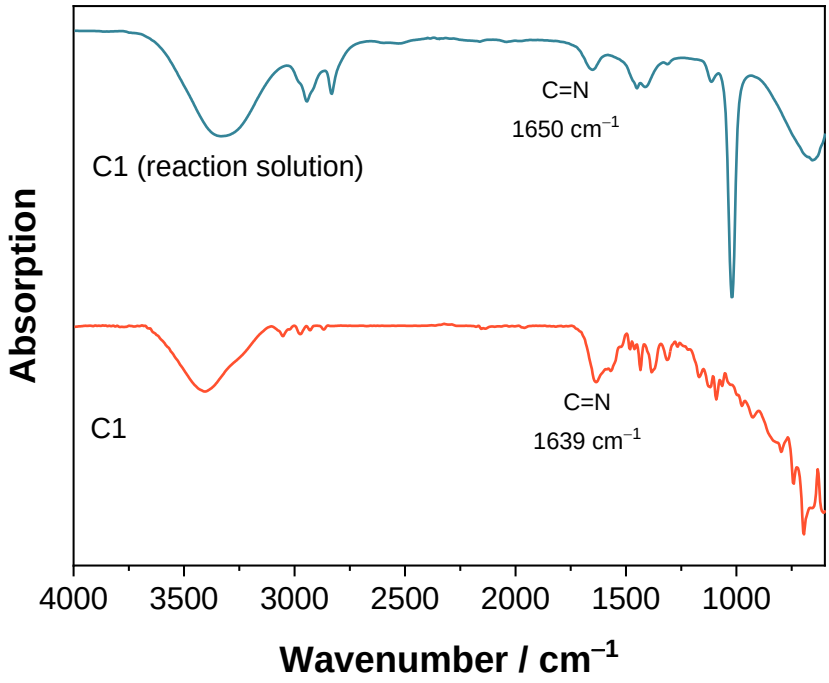

Figure S28. IR spectrum of reaction solution using **C1**.

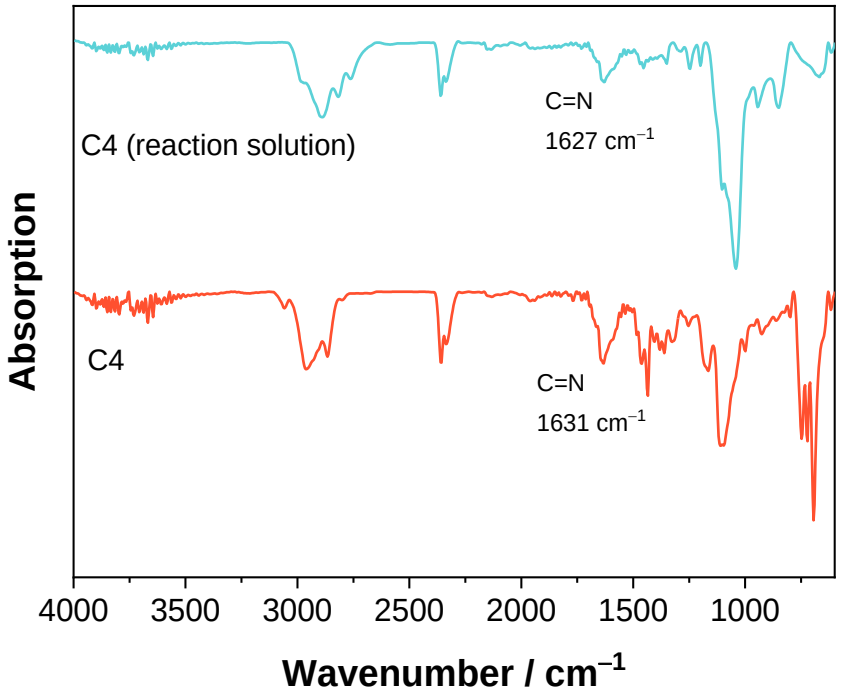

Figure S29. IR spectrum of reaction solution using **C4**.

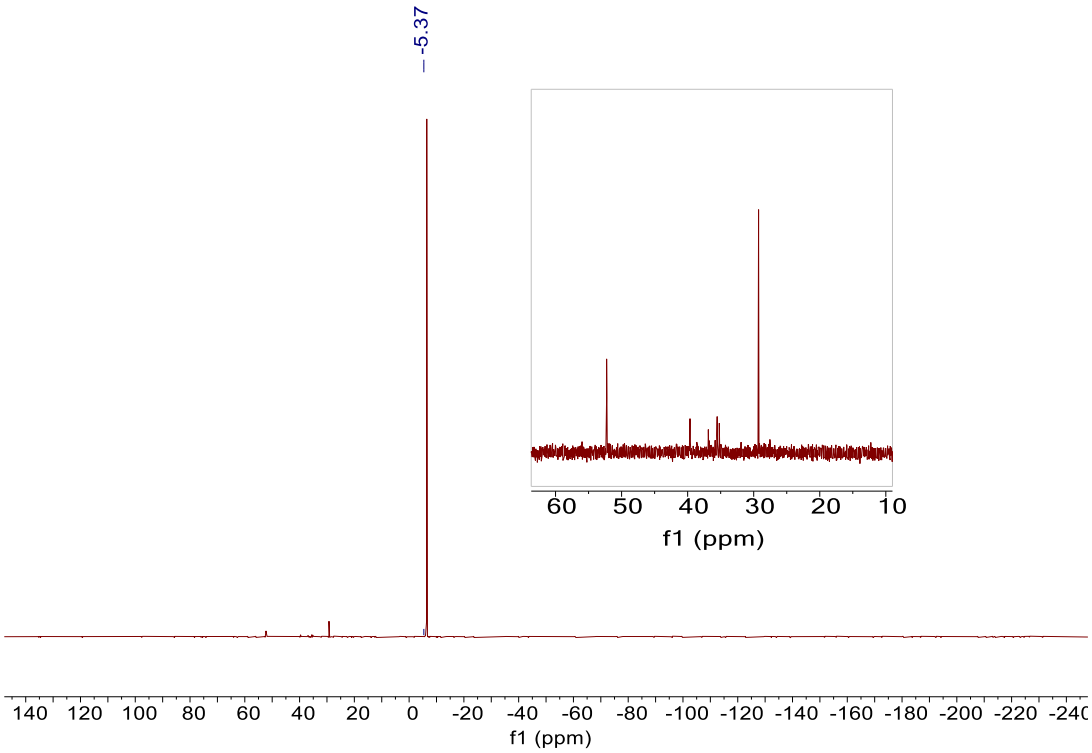

Figure S30. ^{31}P NMR spectrum of reaction solution using **C4** as catalyst.

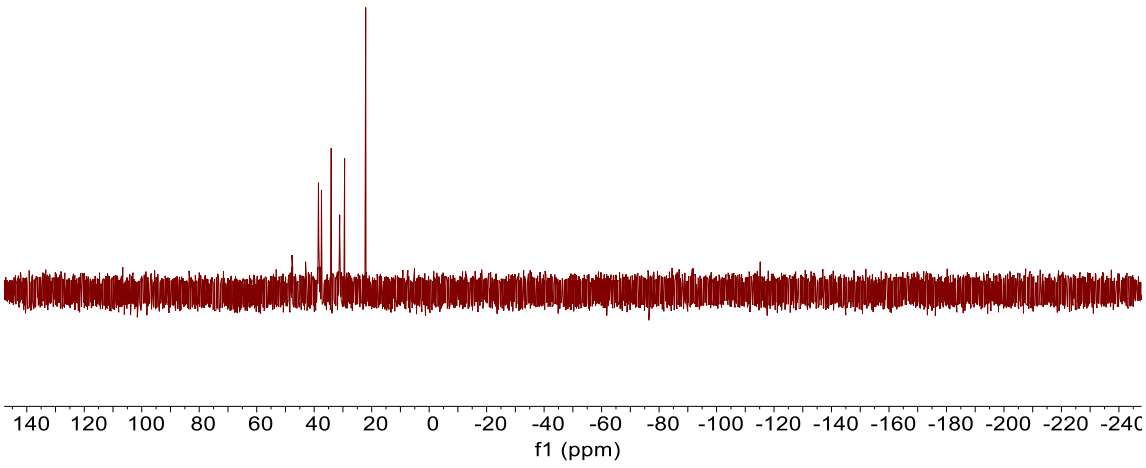

Figure S31. ^{31}P NMR spectrum of reaction solution using **C1** as catalyst.

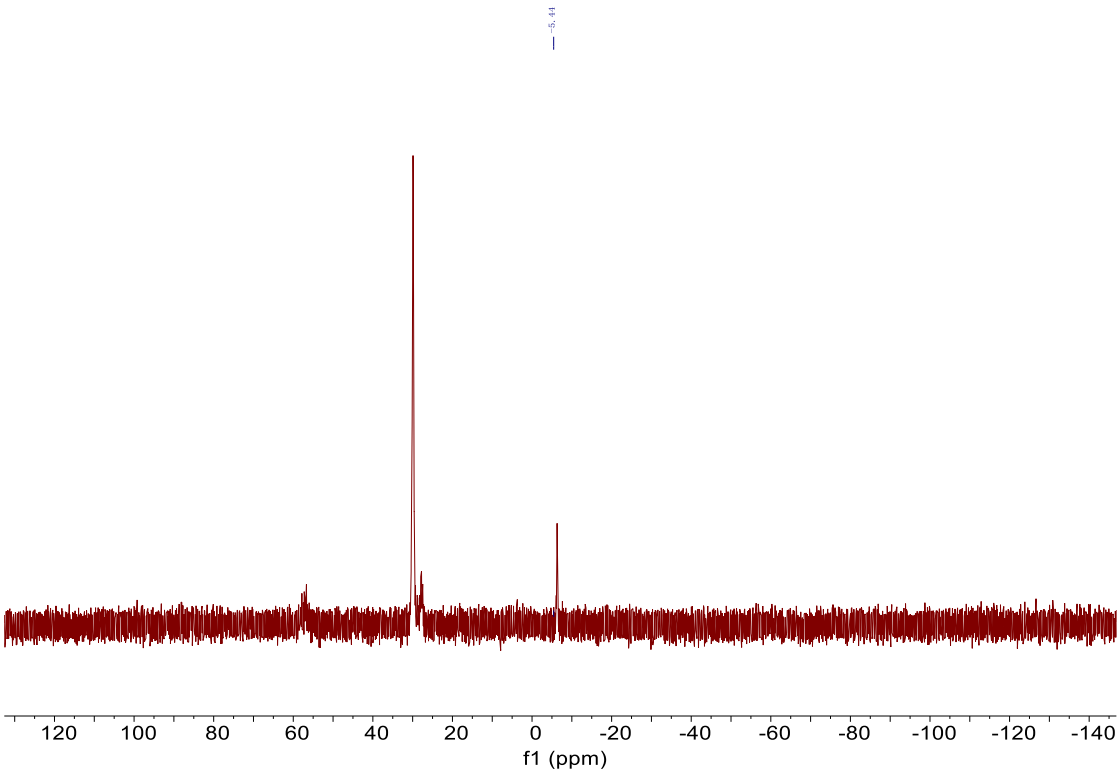

Figure S32. ^{31}P NMR spectrum of reaction solution using **C2** as catalyst.

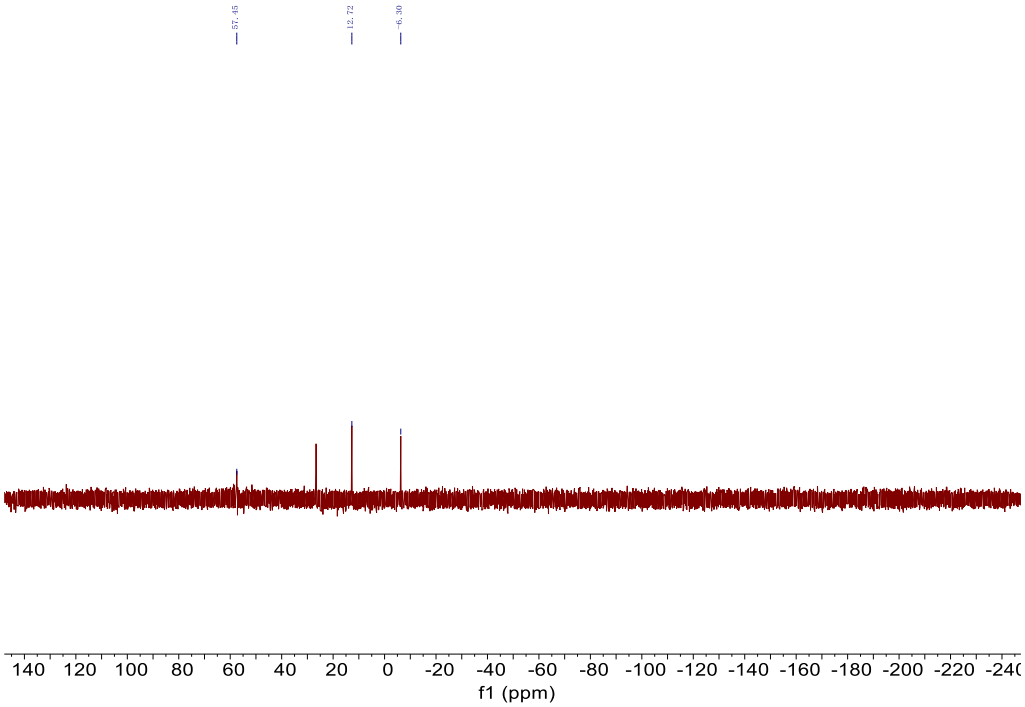

Figure S33. ^{31}P NMR spectrum of reaction solution using **C3** as catalyst.

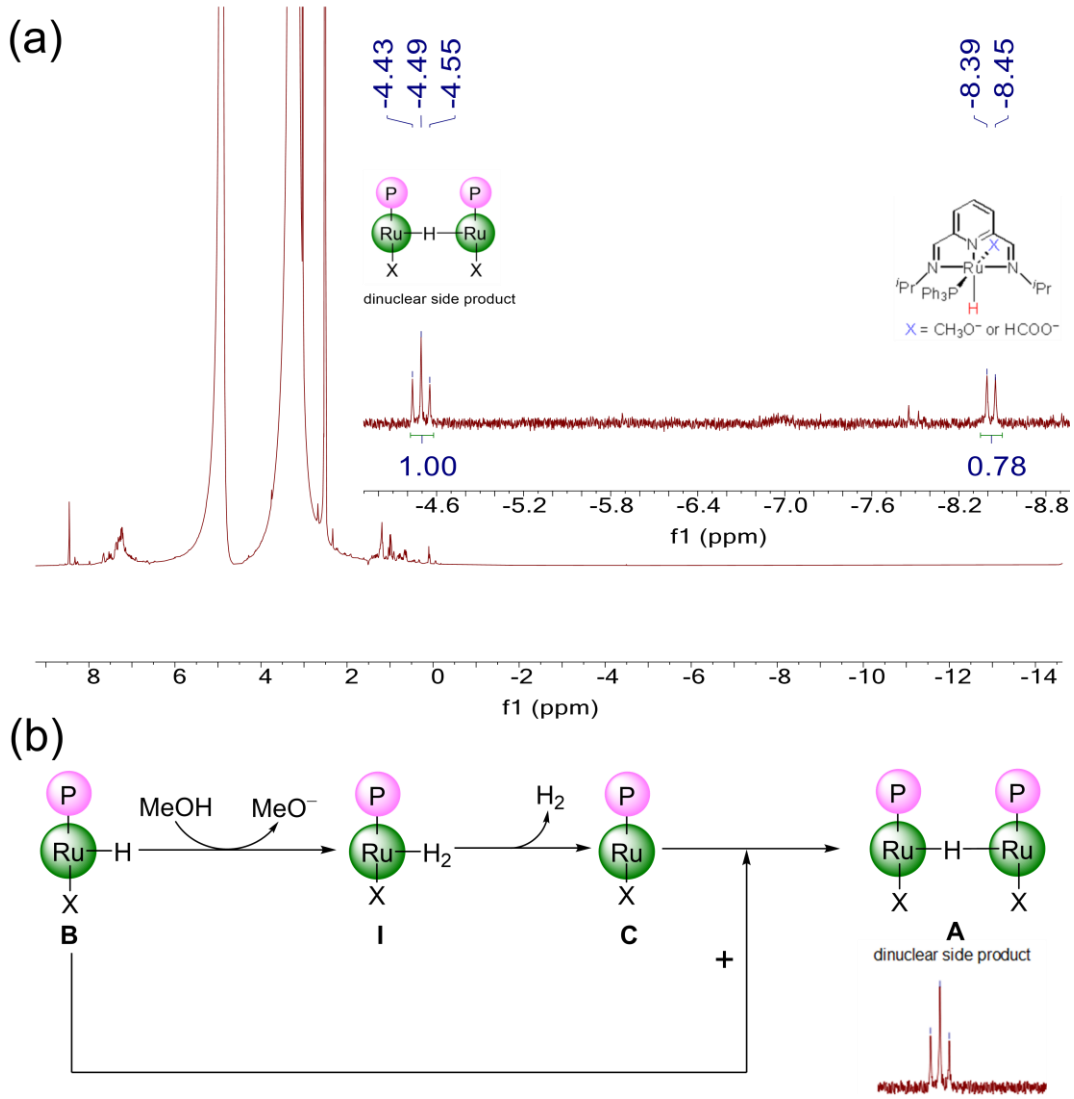

Figure S34. (a) ^{1}H NMR spectrum of reaction solution using **C1** as catalyst (inset: magnified view of the spectral window showing the presence of hydride-containing species); **(b)** A possible route for the formation of the dinuclear species **A** by the aggregation of the catalytically active species **B** (species **c** in Figure 5b in the manuscript) with the pentacoordinate species **C** upon the release of an H_2 molecule from the dihydrogen complex (**I**).

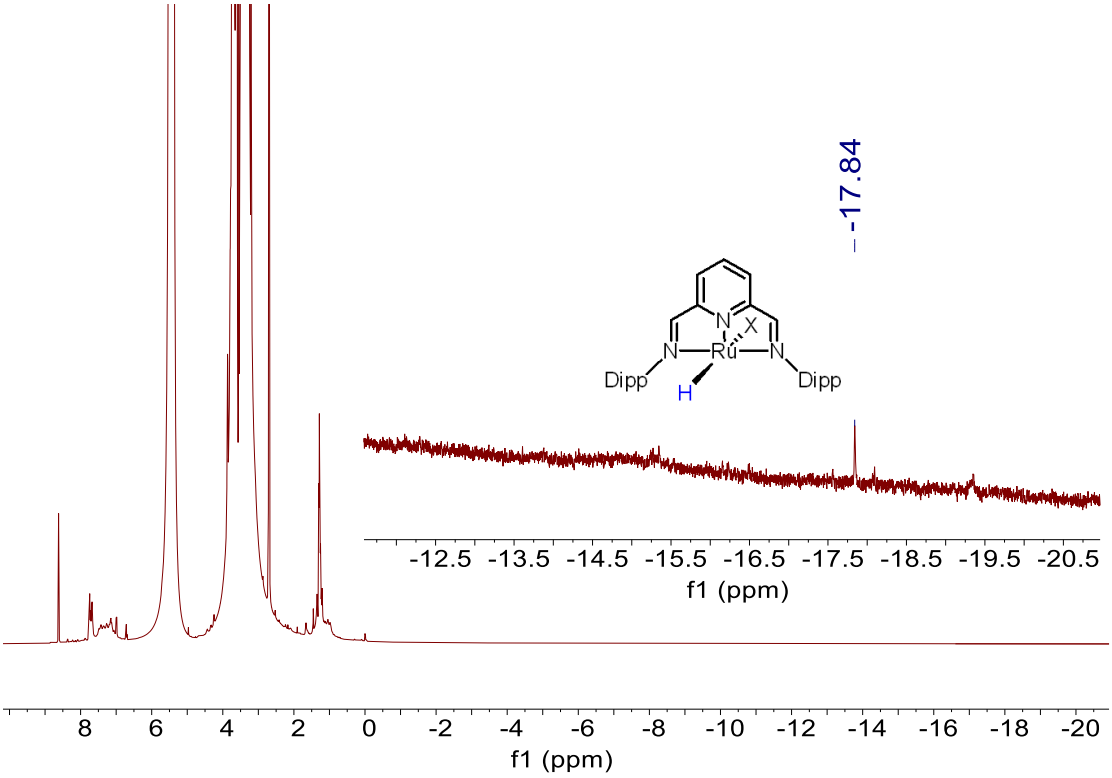

Figure S35. ^{1}H NMR spectrum of reaction solution using **C4** as catalyst.

5. Crystallography Information.

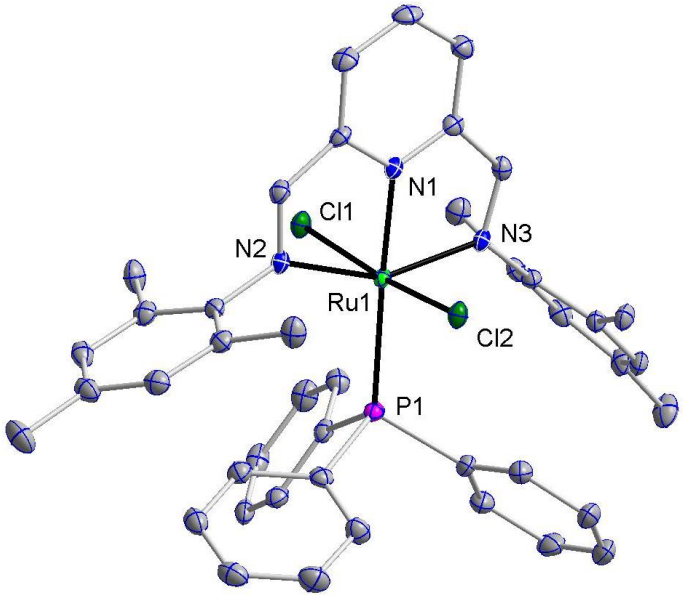

Figure S36. ORTEP diagrams of the molecular structures of **C3**.

Table S1. Crystal data and structure refinement for **C3**.

Identification code	**C3**
Empirical formula	$C_{45}H_{50}Cl_2N_3O_2PRu$
Formula weight	867.82
Temperature/K	100.01
Crystal system	monoclinic
Space group	$P2_1/c$
a/Å	20.9459(13)
b/Å	14.1401(9)
c/Å	14.5156(9)
α/°	90
β/°	109.756(2)
γ/°	90
Volume/Å^3	4046.1(4)
Z	4
ρ_{calc}g/cm^3	1.425
μ/mm^{-1}	0.601
F(000)	1800.0
Crystal size/mm^3	0.217 × 0.191 × 0.065
Radiation	Mo$K\alpha$ (λ = 0.71073)
2Θ range for data collection/°	5.038 to 55.32
Index ranges	$-27 \leq h \leq 27$, $-18 \leq k \leq 18$, $-18 \leq l \leq 18$
Reflections collected	127394
Independent reflections	9390 [R_{int} = 0.0757, R_{sigma} = 0.0304]
Data/restraints/parameters	9390/0/496
Goodness-of-fit on F^2	1.127
Final R indexes [I>=2σ (I)]	R_1 = 0.0491, wR_2 = 0.1108
Final R indexes [all data]	R_1 = 0.0571, wR_2 = 0.1156
Largest diff. peak/hole / e Å^{-3}	3.38/-1.25

Table S2. Bond Lengths for **C3**.

Atom	Atom	Length/Å	Atom	Atom	Length/Å
Ru1	Cl1	2.3995(8)	C2	C3	1.400(5)
Ru1	Cl2	2.3987(8)	C3	C6	1.451(5)
Ru1	P1	2.4007(8)	C7	C14	1.402(4)
Ru1	N1	1.993(3)	C7	C8	1.402(4)
Ru1	N2	2.223(3)	C14	C15	1.513(4)
Ru1	N3	2.102(3)	C14	C13	1.397(5)
P1	C38	1.851(3)	C13	C11	1.392(5)
P1	C26	1.847(4)	C11	C12	1.509(5)
P1	C32	1.847(3)	C11	C10	1.388(5)
O1	C2S	1.402(6)	C10	C8	1.400(5)
O2	C1S	1.399(5)	C8	C9	1.513(5)
N1	C4	1.346(4)	C38	C43	1.401(5)
N1	C3	1.342(4)	C38	C39	1.403(5)
N2	C16	1.297(4)	C43	C42	1.393(5)
N2	C17	1.470(4)	C42	C41	1.387(6)
N3	C6	1.305(4)	C41	C40	1.389(6)
N3	C7	1.455(4)	C40	C39	1.397(5)
C4	C16	1.457(5)	C26	C27	1.391(5)
C4	C5	1.392(4)	C26	C31	1.403(5)
C17	C18	1.404(5)	C27	C28	1.396(5)
C17	C24	1.402(5)	C28	C29	1.386(6)
C18	C20	1.400(5)	C29	C30	1.383(6)
C18	C19	1.504(5)	C30	C31	1.392(5)
C20	C21	1.391(5)	C32	C37	1.402(5)
C21	C22	1.510(5)	C32	C33	1.393(5)
C21	C23	1.393(5)	C37	C36	1.391(5)
C23	C24	1.402(5)	C36	C35	1.383(5)
C24	C25	1.503(5)	C35	C34	1.386(5)
C5	C1	1.386(5)	C34	C33	1.390(5)
C1	C2	1.388(5)			

Table S3. Bond Angles for **C3**.

Atom	Atom	Atom	Angle/°	Atom	Atom	Atom	Angle/°
Cl1	Ru1	P1	96.87(3)	C23	C24	C25	119.6(3)
Cl2	Ru1	Cl1	171.62(3)	C1	C5	C4	118.5(3)
Cl2	Ru1	P1	90.68(3)	C5	C1	C2	120.3(3)
N1	Ru1	Cl1	85.08(8)	C1	C2	C3	118.4(3)
N1	Ru1	Cl2	87.46(8)	N1	C3	C2	120.9(3)
N1	Ru1	P1	177.64(8)	N1	C3	C6	111.9(3)
N1	Ru1	N2	76.96(11)	C2	C3	C6	127.1(3)
N1	Ru1	N3	77.32(11)	N3	C6	C3	117.7(3)
N2	Ru1	Cl1	86.10(7)	C14	C7	N3	119.2(3)
N2	Ru1	Cl2	88.50(7)	C14	C7	C8	120.7(3)
N2	Ru1	P1	104.46(7)	C8	C7	N3	120.1(3)
N3	Ru1	Cl1	89.87(7)	C7	C14	C15	121.6(3)
N3	Ru1	Cl2	92.22(7)	C13	C14	C7	118.1(3)
N3	Ru1	P1	101.30(8)	C13	C14	C15	120.0(3)
N3	Ru1	N2	154.22(10)	C11	C13	C14	122.4(3)
C38	P1	Ru1	118.44(11)	C13	C11	C12	120.9(3)
C26	P1	Ru1	115.52(11)	C10	C11	C13	117.7(3)
C26	P1	C38	101.85(15)	C10	C11	C12	121.3(3)
C32	P1	Ru1	117.00(11)	C11	C10	C8	122.1(3)
C32	P1	C38	99.89(15)	C7	C8	C9	123.2(3)
C32	P1	C26	101.32(15)	C10	C8	C7	118.4(3)
C4	N1	Ru1	120.0(2)	C10	C8	C9	118.3(3)
C3	N1	Ru1	119.3(2)	C43	C38	P1	122.0(3)
C3	N1	C4	120.7(3)	C43	C38	C39	118.5(3)
C16	N2	Ru1	110.3(2)	C39	C38	P1	119.6(3)
C16	N2	C17	111.5(3)	C42	C43	C38	120.8(3)
C17	N2	Ru1	138.2(2)	C41	C42	C43	120.4(4)
C6	N3	Ru1	113.7(2)	C42	C41	C40	119.5(3)
C6	N3	C7	114.5(3)	C41	C40	C39	120.5(4)
C7	N3	Ru1	131.8(2)	C40	C39	C38	120.3(3)
N1	C4	C16	113.0(3)	C27	C26	P1	124.0(3)

(to be continued)

N1	C4	C5	121.2(3)	C27	C26	C31	118.2(3)
C5	C4	C16	125.8(3)	C31	C26	P1	117.8(3)
N2	C16	C4	119.8(3)	C26	C27	C28	120.7(4)
C18	C17	N2	120.1(3)	C29	C28	C27	120.3(4)
C24	C17	N2	118.5(3)	C30	C29	C28	119.8(3)
C24	C17	C18	121.2(3)	C29	C30	C31	120.1(3)
C17	C18	C19	122.8(3)	C30	C31	C26	120.9(3)
C20	C18	C17	118.1(3)	C37	C32	P1	122.8(3)
C20	C18	C19	119.2(3)	C33	C32	P1	118.4(3)
C21	C20	C18	122.4(3)	C33	C32	C37	118.6(3)
C20	C21	C22	121.4(3)	C36	C37	C32	120.5(3)
C20	C21	C23	118.0(3)	C35	C36	C37	120.0(3)
C23	C21	C22	120.6(3)	C36	C35	C34	120.3(3)
C21	C23	C24	122.0(3)	C35	C34	C33	119.7(3)
C17	C24	C23	118.3(3)	C34	C33	C32	120.9(3)
C17	C24	C25	122.0(3)				

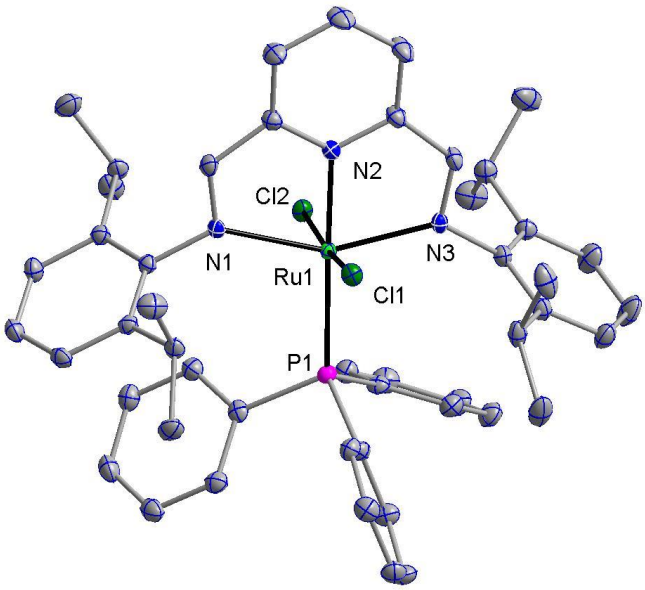

Figure S37. ORTEP diagrams of the molecular structures of **C4**.

Table S4. Crystal data and structure refinement for **C4**.

Identification code	**C4**
Empirical formula	$C_{50}H_{56}Cl_4N_3PRu$
Formula weight	972.81
Temperature/K	100.0
Crystal system	triclinic
Space group	*P*-1
a/Å	10.8192(6)
b/Å	12.7886(7)
c/Å	17.5557(8)
α/°	98.8008(17)
β/°	100.834(3)
γ/°	92.670(2)
Volume/Å^3	2350.6(2)
Z	2
ρ_{calc}g/cm^3	1.374
μ/mm^{-1}	0.632
F(000)	1008.0
Crystal size/mm^3	0.202 × 0.127 × 0.068
Radiation	Mo*K*α (λ = 0.71073)
2Θ range for data collection/°	4.79 to 55.016
Index ranges	$-14 \le h \le 14$, $-16 \le k \le 16$, $-22 \le l \le 22$
Reflections collected	78585
Independent reflections	10777 [R_{int} = 0.0509, R_{sigma} = 0.0285]
Data/restraints/parameters	10777/0/540
Goodness-of-fit on F^2	1.041
Final R indexes [I>=2σ (I)]	R_1 = 0.0303, wR_2 = 0.0736
Final R indexes [all data]	R_1 = 0.0356, wR_2 = 0.0767
Largest diff. peak/hole / e Å^{-3}	1.24/-0.97

Table S5. Bond Lengths for **C4**.

Atom	Atom	Length/Å	Atom	Atom	Length/Å
Ru1	Cl1	2.4241(5)	C20	C21	1.408(3)
Ru1	Cl2	2.3993(5)	C20	C28	1.411(3)
Ru1	P1	2.4300(5)	C21	C22	1.527(3)
Ru1	N1	2.1624(15)	C21	C25	1.398(3)
Ru1	N2	1.9891(15)	C22	C23	1.532(3)
Ru1	N3	2.1415(15)	C22	C24	1.535(3)
P1	C32	1.8528(19)	C25	C26	1.387(3)
P1	C38	1.8465(19)	C26	C27	1.386(3)
P1	C44	1.8565(19)	C27	C28	1.392(3)
N1	C9	1.458(2)	C28	C29	1.517(3)
N1	C13	1.299(2)	C29	C30	1.541(3)
N2	C14	1.345(2)	C29	C31	1.529(3)
N2	C18	1.347(2)	C32	C33	1.406(3)
N3	C19	1.301(2)	C32	C37	1.398(3)
N3	C20	1.458(2)	C33	C34	1.394(3)
C1	C2	1.526(3)	C34	C35	1.385(3)
C2	C3	1.541(3)	C35	C36	1.390(3)
C2	C4	1.514(3)	C36	C37	1.390(3)
C4	C5	1.396(3)	C38	C39	1.403(3)
C4	C9	1.407(3)	C38	C43	1.394(3)
C5	C6	1.386(3)	C39	C40	1.395(3)
C6	C7	1.384(3)	C40	C41	1.392(3)
C7	C8	1.400(3)	C41	C42	1.388(3)
C8	C9	1.407(3)	C42	C43	1.394(3)
C8	C10	1.528(3)	C44	C45	1.402(3)
C10	C11	1.537(3)	C44	C49	1.396(3)
C10	C12	1.536(3)	C45	C46	1.390(3)
C13	C14	1.449(3)	C46	C47	1.390(3)
C14	C15	1.393(3)	C47	C48	1.389(3)
C15	C16	1.394(3)	C48	C49	1.401(3)
C16	C17	1.388(3)	Cl1S	C1S	1.747(3)
C17	C18	1.393(3)	Cl2S	C1S	1.768(3)
C18	C19	1.449(3)			

Table S6. Bond Angles for **C4**.

Atom	Atom	Atom	Angle/°	Atom	Atom	Atom	Angle/°
Cl1	Ru1	P1	99.644(16)	C15	C14	C13	126.74(18)
Cl2	Ru1	Cl1	172.345(16)	C14	C15	C16	118.55(19)
Cl2	Ru1	P1	87.958(16)	C17	C16	C15	119.54(18)
N1	Ru1	Cl1	89.23(4)	C16	C17	C18	119.07(19)
N1	Ru1	Cl2	87.98(4)	N2	C18	C17	121.04(18)
N1	Ru1	P1	104.40(4)	N2	C18	C19	112.02(16)
N2	Ru1	Cl1	80.22(5)	C17	C18	C19	126.93(18)
N2	Ru1	Cl2	92.20(5)	N3	C19	C18	119.06(17)
N2	Ru1	P1	178.66(5)	C21	C20	N3	118.93(16)
N2	Ru1	N1	76.93(6)	C21	C20	C28	122.10(17)
N2	Ru1	N3	77.56(6)	C28	C20	N3	118.73(17)
N3	Ru1	Cl1	89.20(4)	C20	C21	C22	123.51(18)
N3	Ru1	Cl2	90.22(4)	C25	C21	C20	117.37(18)
N3	Ru1	P1	101.11(4)	C25	C21	C22	119.12(18)
N3	Ru1	N1	154.34(6)	C21	C22	C23	111.64(17)
C32	P1	Ru1	116.86(6)	C21	C22	C24	111.14(17)
C32	P1	C44	100.17(8)	C23	C22	C24	110.72(18)
C38	P1	Ru1	121.57(6)	C26	C25	C21	121.5(2)
C38	P1	C32	99.56(9)	C27	C26	C25	119.9(2)
C38	P1	C44	102.49(9)	C26	C27	C28	121.34(19)
C44	P1	Ru1	113.05(6)	C20	C28	C29	120.96(17)
C9	N1	Ru1	135.03(12)	C27	C28	C20	117.77(18)
C13	N1	Ru1	111.69(12)	C27	C28	C29	121.20(18)
C13	N1	C9	112.93(15)	C28	C29	C30	110.11(17)
C14	N2	Ru1	119.77(12)	C28	C29	C31	113.55(18)
C14	N2	C18	120.28(16)	C31	C29	C30	110.10(18)
C18	N2	Ru1	119.03(13)	C33	C32	P1	122.48(15)
C19	N3	Ru1	111.86(12)	C37	C32	P1	119.17(14)
C19	N3	C20	112.05(15)	C37	C32	C33	118.23(18)
C20	N3	Ru1	136.00(12)	C34	C33	C32	120.16(19)
C1	C2	C3	109.31(17)	C35	C34	C33	120.94(19)

(to be continued)

C4	C2	C1	113.70(17)	C34	C35	C36	119.22(19)
C4	C2	C3	109.36(16)	C37	C36	C35	120.34(19)
C5	C4	C2	121.01(17)	C36	C37	C32	121.03(18)
C5	C4	C9	117.97(17)	C39	C38	P1	122.13(15)
C9	C4	C2	120.70(16)	C43	C38	P1	119.12(14)
C6	C5	C4	121.28(18)	C43	C38	C39	118.21(17)
C7	C6	C5	119.73(18)	C40	C39	C38	120.72(19)
C6	C7	C8	121.57(18)	C41	C40	C39	120.31(18)
C7	C8	C9	117.55(17)	C42	C41	C40	119.37(18)
C7	C8	C10	118.21(17)	C41	C42	C43	120.32(19)
C9	C8	C10	124.23(17)	C38	C43	C42	121.05(18)
C4	C9	N1	118.68(16)	C45	C44	P1	120.21(15)
C8	C9	N1	119.38(16)	C49	C44	P1	121.62(15)
C8	C9	C4	121.86(17)	C49	C44	C45	118.15(18)
C8	C10	C11	110.56(17)	C46	C45	C44	120.71(19)
C8	C10	C12	111.13(16)	C47	C46	C45	120.33(19)
C12	C10	C11	110.28(17)	C48	C47	C46	120.0(2)
N1	C13	C14	119.19(17)	C47	C48	C49	119.3(2)
N2	C14	C13	111.79(16)	C44	C49	C48	121.40(19)
N2	C14	C15	121.47(17)	Cl1S	C1S	Cl2S	112.01(16)

6. Supporting references.

S1. Dolomanov, O. V.; Bourhis, L. J.; Gildea, R. J.; Howard, J. A. K.; Puschmann, H. OLEX2: A complete structure solution, refinement and analysis program. *J. Appl. Crystallogr.* **2009**, *42*, 339–341.

S2. Sheldrick, G. M. SHELXT–Integrated space-group and crystal-structure determination. *Acta Crystallogr., Sect. A: Found. Adv.* **2015**, *71*, 3–8.

S3. Sheldrick, G. M. Crystal structure refinement with SHELXL. *Acta Crystallogr., Sect. C: Struct. Chem.* **2015**, *71*, 3–8.

S4. Das, K., Dutta, M., Das, B., Srivastava, H. K., Kumara, A., Efficient Pincer-Ruthenium Catalysts for Kharasch Addition of Carbon Tetrachloride to Styrene. *Adv. Synth. Catal.* **2019,** *361*, 2965–2980.

S5. Garza-Ortiz, A., Maheswari, P. U., Lutz, M., Siegler, M. A., Reedijk, J. Tuning the cytotoxic properties of new ruthenium(III) and ruthenium(II) complexes with a modified bis(arylimino)pyridine Schiff base ligand using bidentate pyridine-based ligands. *J. Biol. Inorg. Chem.* **2014**, *19*, 675–689.

S6. Garza-Ortiz, A., Maheswari, P. U., Siegler, M., Spek, A. L. Reedijk, J. Ruthenium(III) Chloride Complex with a Tridentate Bis(arylimino)pyridineLigand: Synthesis, Spectrum, X-ray Structure, 9-Ethylguanine BindingPattern, and In Vitro Cytotoxicity. *Inorg. Chem*. **2008**, *47*, 6964–6973.

S7. Dutta, M., Das, K., Prathapa, S. J., Srivastava, H. K., Kumar, A. Selective and high yield transformation of glycerol to lactic acid using NNN pincer ruthenium catalysts. *Chem. Commun.* **2020**, *56*, 9886–9889.